Design, Synthesis, and Characterization of Novel Iron Chelators: Structure−Activity Relationships of the 2-Benzoylpyridine Thiosemicarbazone Series and Their 3-Nitrobenzoyl Analogues as Potent Antitumor Agents

Danuta S. Kalinowski,[†] Yu Yu,[†] Philip C. Sharpe,[‡] Mohammad Islam,[‡] Yi-Tyng Liao,[§] David B. Lovejoy,[†] Naresh Kumar,[§] Paul V. Bernhardt,*[,‡] and Des R. Richardson*[,†]

Iron Metabolism and Chelation Program, Department of Pathology, University of Sydney, Sydney, New South Wales 2006, Australia, Centre for Metals in Biology, Department of Chemistry, University of Queensland, Brisbane, Queensland 4072, Australia, and School of Chemistry, University of New South Wales, Sydney, New South Wales 2052, Australia.

Received April 16, 2007

Previously, we demonstrated that the potent antiproliferative activity of the di-2-pyridylketone thiosemicarbazone (DpT) series of Fe chelators was due to their ability to induce Fe depletion and form redox-active Fe complexes (Richardson, D. R.; et al. *J. Med. Chem*. **2006**, *49*, 6510−6521). We now examine the role of aromatic substituents on the antiproliferative and redox activity of novel DpT analogues, namely, the 2-benzoylpyridine thiosemicarbazone (BpT) and 2-(3-nitrobenzoyl)pyridine thiosemicarbazone (NBpT) series. Both series exhibited selective antiproliferative effects, with the majority having greater antineoplastic activity than their DpT homologues. This makes the BpT chelators the most active anticancer agents developed within our laboratory. The BpT series Fe complexes exhibit lower redox potentials than their corresponding DpT and NBpT complexes, highlighting their enhanced redox activity. The increased ability of BpT-Fe complexes to catalyze ascorbate oxidation and benzoate hydroxylation, relative to their DpT and NBpT analogues, suggested that redox cycling plays an important role in their antiproliferative activity.

Introduction

Traditionally, iron (Fe) chelators were developed for the treatment of Fe overload disease[1−3] and their use in cancer chemotherapy represents a novel avenue of investigation.[4−7] The increased requirement for Fe in rapidly proliferating cancer cells, compared with normal cells, is illustrated by the increased expression of transferrin receptor 1 (TfR1).[8] This membrane protein is necessary for Fe uptake from the serum Fe-transport protein, transferrin (Tf[a]).[8]

Iron chelators can remove Fe from biological systems and are able to inhibit the activity of Fe-requiring proteins, including ribonucleotide reductase, a key enzyme involved in the rate-limiting step of DNA synthesis.[9−11] However, the antiproliferative activity of Fe chelators is probably mediated by their effects on multiple molecular targets.[12−14] Chelators with potent antiproliferative activity also demonstrate the ability to form Fe complexes that redox cycle.[10,15−19] This leads to the generation of reactive oxygen species (ROS) such as hydroxyl radicals ($OH^{\bullet}$), which induce cellular injury, including DNA oxidation and mitochondrial damage.[10,15−19]

Previous studies using the Fe chelator desferrioxamine (DFO, Figure 1A) demonstrated only modest antitumor efficacy in vitro and in vivo.[4,15] In fact, the poor membrane permeability of DFO limited its activity and application in cancer therapy.[20,21] This has led to research examining novel Fe chelators as cancer chemotherapeutics.[22−25] For example, more hydrophobic Fe chelators, such as 3-aminopyridine-2-carboxaldehyde thiosemicarbazone (3-AP, Figure 1A), have been investigated as potential anticancer therapeutics (for reviews, see refs 4 and 15).

Chelators previously developed within our laboratory, namely, the di-2-pyridyl ketone isonicotinoyl hydrazone (PKIH) series (Figure 1B), exhibited moderate antiproliferative activity against the SK-N-MC neuroepithelioma cell line.[26,27] These ligands were able to stimulate benzoate hydroxylation in the presence of Fe^{II} and H_2O_2.[16] Furthermore, $Fe^{II}(PKIH)_2$ complexes were found to enhance DNA plasmid degradation in the presence of H_2O_2.[27] Cyclic voltammetry of the $Fe^{II}(PKIH)_2$ complexes revealed their complicated (irreversible) electrochemistry.[27] Indeed, the complex underwent rapid nucleophilic attack by hydroxide on the imine C-atom upon oxidation to Fe^{III} (i.e., from $-C{=}N-Fe^{III}$ to $-C(OH)-N-Fe^{III}$). Importantly, subsequent reduction of this carbinolamine ($-C(OH)-N-Fe^{III}$) form to the ferrous oxidation state occurred at a much lower potential.[27] Hence, the potentially strong oxidizing power of the $[Fe^{III}(PKIH)_2]^+$ complexes was quenched by this chemical reaction.[27] These results suggested that redox cycling played a part in the cytotoxicity of the PKIH analogues.

* To whom correspondence should be addressed. For P.V.B.: phone, +61-7-3365-4266; fax, +61-7-3365-4299; e-mail, p.bernhardt@uq.edu.au. For D.R.R.: phone, +61-2-9036-6548; fax, +61-2-9036-6549; e-mail, d.richardson@med.usyd.edu.au.

[†] University of Sydney.

[‡] University of Queensland.

[§] University of New South Wales.

[a] Abbreviations: 3-AP, 3-aminopyridine-2-carboxaldehyde thiosemicarbazone; DFO, desferrioxamine; BpT, 2-benzoylpyridine thiosemicarbazone; Bp4aT, 2-benzoylpyridine 4-allyl-3-thiosemicarbazone; Bp4eT, 2-benzoylpyridine 4-ethyl-3-thiosemicarbazone; Bp44mT, 2-benzoylpyridine 4,4-dimethyl-3-thiosemicarbazone; Bp4mT, 2-benzoylpyridine 4-methyl-3-thiosemicarbazone; Bp4pT, 2-benzoylpyridine 4-phenyl-3-thiosemicarbazone; DpT, di-2-pyridylketone thiosemicarbazone; Dp44mT, di-2-pyridylketone 4,4-dimethyl-3-thiosemicarbazone; IBE, iron-binding equivalent; NBpT, 2-(3-nitrobenzoyl)pyridine thiosemicarbazone; NBp4aT, 2-(3-nitrobenzoyl)-pyridine 4-allyl-3-thiosemicarbazone; NBp4eT, 2-(3-nitrobenzoyl)pyridine 4-ethyl-3-thiosemicarbazone; NBp44mT, 2-(3-nitrobenzoyl)pyridine 4,4-dimethyl-3-thiosemicarbazone; NBp4mT, 2-(3-nitrobenzoyl)pyridine 4-methyl-3-thiosemicarbazone; NBp4pT, 2-(3-nitrobenzoyl)pyridine 4-phenyl-3-thiosemicarbazone; NIH, 2-hydroxy-1-naphthaldehyde isonicotinoyl hydrazone; PIH, pyridoxal isonicotinoyl hydrazone; PKBH, di-2-pyridylketone benzoyl hydrazone; PKIH, di-2-pyridylketone isonicotinoyl hydrazone; ROS, reactive oxygen species; Tf, transferrin.

10.1021/jm070445z CCC: $37.00
Published on Web 06/30/2007

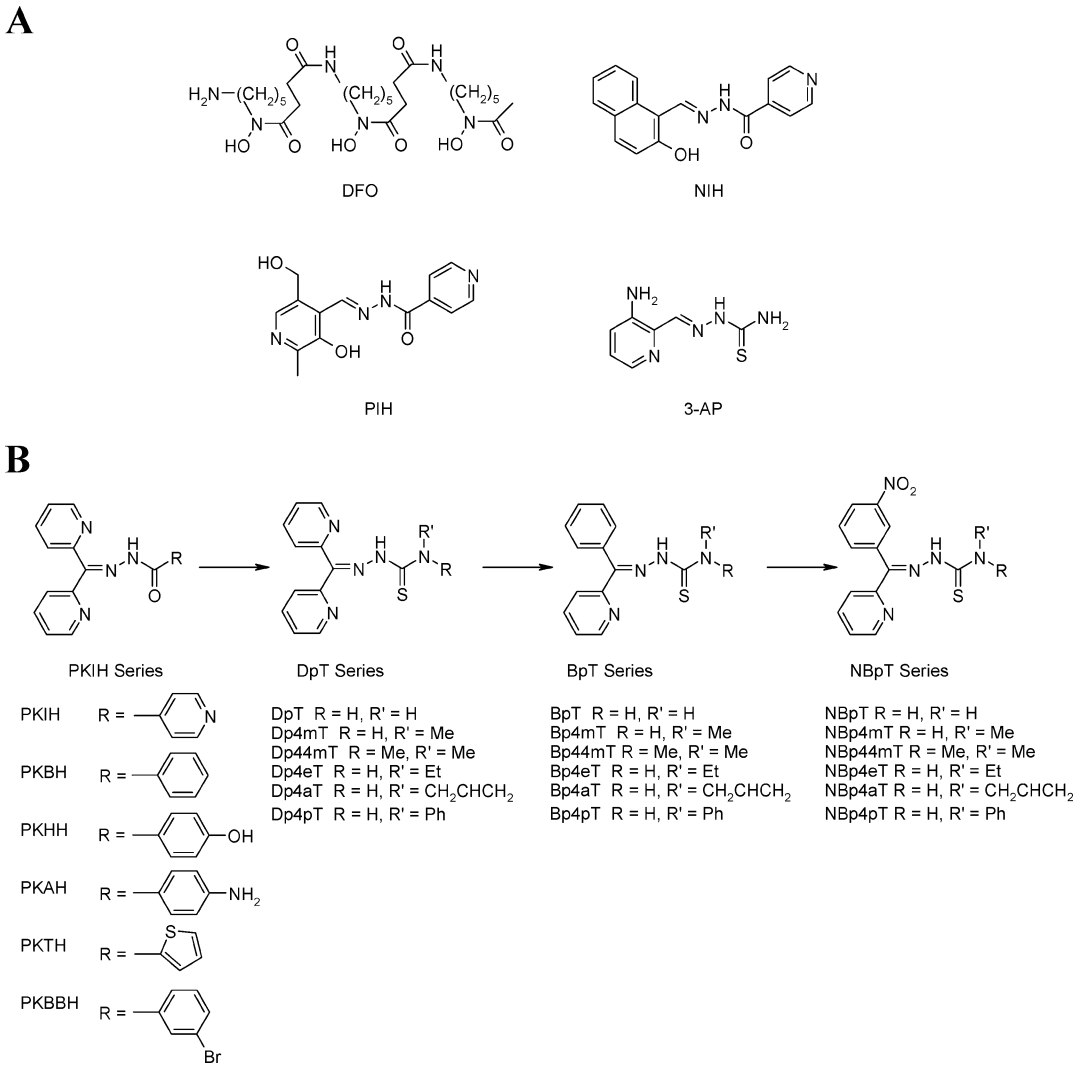

Figure 1. (A) Chemical structures of the iron chelators desferrioxamine (DFO), 2-hydroxy-1-naphthaldehyde isonicotinoyl hydrazone (NIH), pyridoxal isonicotinoyl hydrazone (PIH), and 3-aminopyridine-2-carboxaldehyde thiosemicarbazone (3-AP). (B) Chemical structures of members of the di-2-pyridylketone isonicotinoyl hydrazone (PKIH) series, di-2-pyridylketone thiosemicarbazone (DpT) series, 2-benzoylpyridine thiosemicarbazone (BpT) series, and 2-(3-nitrobenzoyl)pyridine thiosemicarbazone (NBpT) series, illustrating the sequence in which they were developed.

In an effort to develop increasingly active but selective antiproliferative agents, a series of PKIH derivatives were designed to incorporate the thiosemicarbazone moiety.[17] This gave rise to the di-2-pyridylketone thiosemicarbazone (DpT) series (Figure 1B), which exhibited potent antiproliferative activity.[17] In particular, di-2-pyridylketone 4,4-dimethyl-3-thiosemicarbazone (Dp44mT, Figure 1B) demonstrated the highest activity of all ligands within this series (IC_{50} = 0.03 μM).[17] An in vivo study showed a 50% reduction in growth of a murine M109 lung cancer after 5 days of treatment with Dp44mT while having little effect on hematological indices.[17] In addition, initial studies indicated that the Fe complex was redox-active within cells.[17] More recently, Dp44mT has shown marked and selective activity in vivo against a panel of human tumors in nude mice.[28]

The chemical properties of the DpT series Fe complexes have also been extensively investigated in relation to their biological activity.[29] In contrast to the PKIH series, the electrochemistry of the Fe complexes of the DpT analogues showed facile interconversion between the Fe^{II} and Fe^{III} states.[29] This was confirmed by the isolation of both the $Fe^{II}(DpT)_2$ and $[Fe^{III}(DpT)_2](ClO_4)$ complexes, indicating the stable nature of both the ferric and ferrous states. Furthermore, the $Fe(DpT)_2$ series $Fe^{III/II}$ redox potential (+153 to +225 mV vs NHE) were found to lie within the range accessible to both cellular oxidants and reductants.[29] This suggested that the antitumor activity of these chelators was due to their ability to bind intracellular Fe and form redox-active complexes, inducing oxidative cell damage.[29,30]

In an attempt to gain further insight into chelator structure−activity relationships, in the current study we probed the importance of the noncoordinating 2-pyridyl moiety on the biological activity and Fe coordination chemistry of the DpT analogues. This was done by substituting in place of the 2-pyridyl group either a phenyl ring or a 3-nitrophenyl group to generate the benzoylpyridine thiosemicarbazone (BpT, Figure 1B) or 2-(3-nitrobenzoyl)pyridine thiosemicarbazone (NBpT, Figure 1B) analogues, respectively. Introduction of the strong electron-withdrawing nitro group into the noncoordinating phenyl ring was assessed to determine its affect on antiproliferative activity.

The Fe coordination chemistry, Fe chelation efficacy, redox activity, antiproliferative activity, and thus structure−activity relationships of these novel ligands were then examined in detail. We demonstrated that the 2-benzoylpyridine moiety of the BpT

series enhanced antiproliferative efficacy relative to its DpT homologues and was vital for increased redox-cycling activity.

Results and Discussion

Synthesis of the BpT and NBpT Series Ligands. This study represents the first investigation of the antiproliferative activity of the BpT and NBpT series directly in relation to cellular Fe deprivation and the redox-cycling of the Fe complexes. There is continuing interest in the biological activity of thiosemicarbazones and their complexes.[31−40] A wide spectrum of activity has been reported from various BpT analogues including both the free ligands and their Cu^{II}, Ni^{II}, Zn^{II}, and Sn^{II} complexes, e.g. as antimicrobial[31,32] or antifungal[33−35] agents. Interestingly, the antitumor activity of complexes of BpT, Bp4mT, Bp4eT, and Bp4pT with Cu^{II}, Sn^{II}, and Pd^{II} has been examined.[36,37,39] However, the Fe coordination chemistry of the BpT and NBpT analogues has been largely ignored and their biological activity and antitumor activity are unknown. In fact, no crystal structures of the Fe complexes of the BpT or NBpT series have been determined, and this is necessary in order to further understand their biological effects.

Characterization of the Free Ligands. The ligand syntheses involved relatively straightforward Schiff base condensation reactions and follow previous protocols for related thiosemicarbazones and hydrazones reported from our laboratory.[27,29] One notable exception was NBp44mT (Figure 1B), which required anhydrous conditions to ensure isolation of a pure product. In the presence of water, incomplete reaction (with recovery of starting materials) was a persistent problem. The nitro substituent was evidently responsible for this destabilization because the corresponding Bp44mT homologue was readily synthesized. The electron-withdrawing effect of the nitro substituent made the imine (−N═C(Ph)(Py)) group more susceptible to hydrolysis. Indeed, a reaction time of 4−6 h was necessary for all members of the NBpT series, while shorter reaction times (<1 h) can be employed for the BpT analogues.

The IR and ^{1}H NMR spectral properties of the BpT and NBpT ligands are very similar to those of the DpT analogues,[29] as expected. The NBpT series exhibit a prominent pair of additional IR peaks from the nitro group at ∼1525 cm^{-1} (asymmetric $-NO_2$ stretch) and 1345 cm^{-1} (symmetric $-NO_2$ stretch).

The crystal structure of NBpT was determined (Figure 2A), and crystal data can be found in Table 1. Selected bond lengths and angles are included in Supporting Information. A prominent structural feature of NBpT is the presence of an intramolecular H-bond between the thioamide proton and pyridyl nitrogen with an intramolecular N···H distance of 1.97 Å. This feature is common to other related chelators, including members of the PKIH, DpT, and BpT series, which have been described previously.[27,29,40] An additional intramolecular H-bond is observed between the terminal NH_2 proton and the imine nitrogen with an intramolecular N···H distance of 2.23 Å. This interaction is also evident in the crystal structure of the related chelator, BpT.[40]

Partition Coefficients of the Free Ligands. The octanol−water partition coefficients for both the BpT and NBpT analogues (Table 2) were determined using methods reported previously by our laboratories.[29] This was important, as lipophilicity of chelators is known to be a relevant factor in terms of their antiproliferative activity.[41] The log *P* values varied from 0.74 (Bp4mT) to 4.01 (Bp4eT). Edward et al. reported that the PIH class of chelators have maximum activity at mobilizing Fe from cells when they have values of log *P* of 2.8.[42] Many of the ligands examined in this study have log *P* values within this "optimal" range, which may in part explain their high Fe chelation efficacy and antiproliferative activity (see below). However, there was no consistent trend in log *P* values across the three series that could be associated with a particular terminal (N4) substituent.

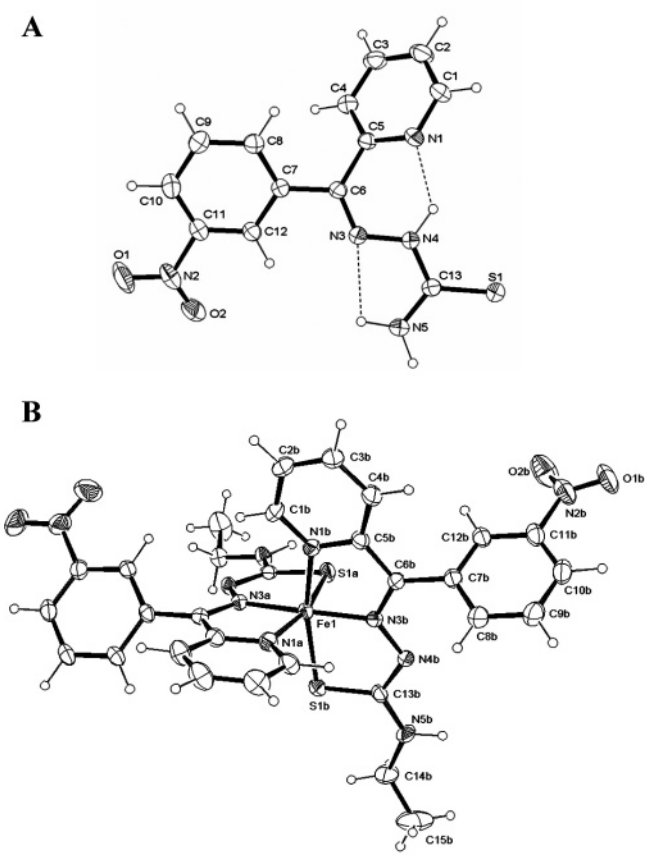

Figure 2. ORTEP diagrams of (A) NBpT and (B) $Fe(NBp4eT)_2$ (30% probability ellipsoid shown).

Table 1. Crystal Data

	NBpT	$Fe^{II}(NBp4eT)_2 \cdot 0.5C_7H_8$
formula	$C_{13}H_{11}N_5O_2S$	$C_{33.5}H_{32}FeN_{10}O_4S_2$
MW	301.3	758.7
crystal system	triclinic	monoclinic
a (Å)	8.416(4)	14.742(5)
b (Å)	8.660(3)	12.615(3)
c (Å)	9.683(3)	20.984(8)
α (deg)	99.09(2)	
β (deg)	92.14(3)	114.60(2)
γ (deg)	90.98(3)	
V (Å^3)	696.2(4)	3548(2)
T (K)	293	293
Z	2	4
space group	$P\bar{1}$	$P2_1/c$
μ(Mo Kα) (mm^{-1})	0.243	0.596
indep reflns (R_{int})	2073 (0.011)	6210 (0.027)
R_1 (obsd data)	0.034	0.052
wR2 (all data)	0.058	0.052
CCDC no.	643 403	643 404

Fe Coordination Chemistry. Both the Fe^{II} and Fe^{III} complexes of each series were isolated and characterized. Their electronic spectral properties mirror those of the respective $Fe^{II}(DpT)_2$ and $[Fe^{III}(DpT)_2]^+$ analogues and are dominated by charge-transfer transitions. The Fe^{II} complexes are invariably an intense green color because of a metal to ligand (Fe^{II} to pyridyl) charge-transfer transition that occurred around 640 nm. The Fe^{III} complexes do not show this band and are very dark-brown.

Table 2. Partition Coefficients, $Fe^{III/II}$ Redox Potentials, and IC_{50} (μM) Values of the DpT, BpT, and NBpT Series Chelators and Their Ferrous and Ferric Complexes at Inhibiting the Growth of SK-N-MC Neuroepithelioma Cells As Determined by the MTT Assay[a]

ligand (L)	partition coefficient (log *P*)	$Fe^{III/II}$ redox potential (mV vs NHE)	IC_{50} (μM) free ligand	$Fe^{II}(L)_2$ complex	$Fe^{III}(L)_2ClO_4$ complex	*p*
DFO			4.51 ± 0.72			
NIH			0.71 ± 0.31			
3-AP			0.26 ± 0.06			
DpT	0.78	+165	3.52 ± 0.35	> 6.25[b]	>6.25[b]	
Dp4mT	3.18	+153	0.27 ± 0.07	1.53 ± 0.21[b]	1.02 ± 0.28[b]	<0.001[b]
Dp44mT	2.19	+166	0.001 ± 0.001	0.42 ± 0.08[b]	0.35 ± 0.02[b]	<0.001[b]
Dp4eT	1.23	+173	0.08 ± 0.01	1.21 ± 0.47[b]	0.46 ± 0.16[b]	<0.001[b]
Dp4aT	1.68	+170	0.05 ± 0.01	0.69 ± 0.24[b]	0.68 ± 0.15[b]	<0.001[b]
Dp4pT	1.96	+225	0.01 ± 0.01	0.21 ± 0.05[b]	0.15 ± 0.09[b]	<0.001[b]
BpT	1.92	+120	4.66 ± 1.59	1.05 ± 0.19	1.17 ± 0.17	<0.05
Bp4mT	0.74	+108	0.004 ± 0.002	0.67 ± 0.08	0.013 ± 0.001	<0.001
Bp44mT	1.29	+119	0.004 ± 0.001	0.21 ± 0.04	0.35 ± 0.08	<0.001
Bp4eT	4.01	+99	0.002 ± 0.001	0.28 ± 0.02	0.40 ± 0.06	<0.001
Bp4aT	2.69	+117	0.004 ± 0.004	0.36 ± 0.05	0.34 ± 0.06	<0.001
Bp4pT	1.92	+180	0.005 ± 0.002	0.21 ± 0.05	0.17 ± 0.01	<0.005
NBpT	1.90	+189	3.82 ± 1.06	>6.25	4.19 ± 0.34	*c*
NBp4mT	2.14	+185	0.13 ± 0.05	0.21 ± 0.11	2.53 ± 0.18	*d*
NBp4eT	2.53	+170	0.014 ± 0.004	2.00 ± 0.25	2.03 ± 0.14	<0.001
NBp4aT	1.70	+187	0.013 ± 0.001	0.20 ± 0.05	1.73 ± 0.22	<0.005
NBp4pT	3.35	+249	0.04 ± 0.01	0.12 ± 0.02	>6.25	<0.001

[a] Cells were seeded and allowed to attach to wells for 24 h and then incubated for 72 h at 37 °C with control medium or the chelators. Results are the mean ± SD (three experiments). The *p* values were determined using Student's *t*-test and were used to compare the activity of the ligand to that of its complex. A value of $p < 0.05$ was considered as significant. Comparable data for DFO, NIH, and 3-AP are also shown. NBp44mT was not included because of instability. [b] IC_{50} data and *p* values previously determined.[29] [c] Ferrous complex, $p < 0.02$; ferric complex, $p > 0.05$. [d] Ferrous complex, $p > 0.05$; ferric complex, $p < 0.001$.

The crystal structure of $Fe^{II}(NBp4eT)_2$ is shown in Figure 2B, and the crystal data set is presented in Table 1. The crystal structure reveals a bis-ligand Fe^{II} complex comprising a N_4S_2 donor set, where each thioamide NH-group (in the 2-position) is deprotonated, forming a charge neutral complex. Charge neutrality is an important characteristic for biological activity, allowing mobilization of intracellular Fe through the cell membrane (see below). This structure shows the complex to have distorted octahedral coordination geometry, with the ligands arranged in a meridional manner, binding through the pyridyl nitrogen (N1A and N1B), imine nitrogen (N3A and N3B), and sulfur (S1A and S1B) atoms. The coordinate bonds vary in length, with the shortest being to the imine nitrogens at ~1.90 Å and the longest being to the sulfur atoms at ~2.28 Å. The crystal structure of the related bis(pyridine-2-carbaldehyde thiosemicarbazone)Fe^{II} complex has been reported, and the bond lengths determined here are similar.[43] Of particular note is the similarity in bond lengths seen in one-electron-oxidized bis(2-pyridyl thiosemicarbazone)Fe^{III} complexes,[44−47] which indicates a very small inner sphere reorganizational energy upon electron transfer.

The low-spin Fe^{II} center in the solid state did not persist in solution, and no NMR spectra of any of the Fe^{II} complexes were obtained because of paramagnetism of the compound. It is most likely that partial oxidation to the ferric form is the origin of this paramagnetism given the low $Fe^{III/II}$ redox potentials (see below), although a high-spin/low-spin equilibrium of the Fe^{II} state cannot be ruled out.

Electrochemistry. The electrochemical properties of the Fe complexes of the BpT and NBpT analogues constituted a crucial part of this study. In fact, it has been suggested that the antiproliferative activity of related chelators reported by us previously is linked to their capability to undergo Fenton chemistry upon complexation with intracellular Fe.[16,27,29] In all cases, totally reversible $Fe^{III/II}$ couples were identified at sweep rates between 50 and 500 mV s^{-1}. The redox potentials of the Fe complexes are collected in Table 2 and may be compared with those of the $Fe(DpT)_2$ analogues.[29] As an example, the cyclic voltammograms of three Fe^{III} complexes, namely, $[Fe(Bp4mT)_2]^+$, $[Fe(Dp4mT)_2]^+$, and $[Fe(NBp4mT)_2]^+$ bearing the same terminal substituent (−NHMe) are shown in Figure 3. This was done to illustrate the inductive effects of the three different noncoordinating aromatic groups on the $Fe^{III/II}$ redox potential. The electron-withdrawing 3-nitrophenyl group (from the NBpT series) leads to the highest $Fe^{III/II}$ couples in each case, followed by the pyridyl (DpT) and phenyl (BpT) analogues.

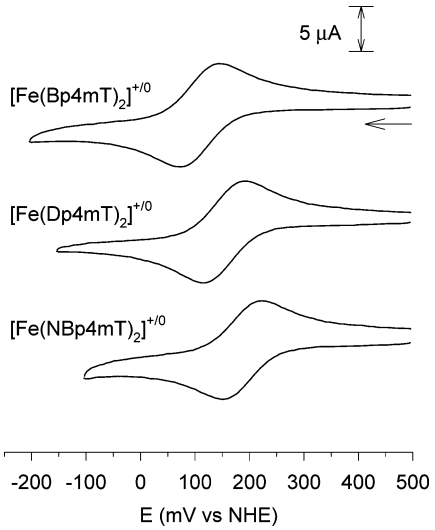

Figure 3. Cyclic voltammograms of 1 mM solutions of $[Fe(Bp4mT)_2]^+$ (top), $[Fe(Dp4mT)_2]^+$ (center), and $[Fe(NBp4mT)_2]^+$ (bottom) showing the increasing electron-withdrawing effects of the phenyl, pyridyl, and 3-nitrophenyl substituents in raising the $Fe^{III/II}$ redox potential. The parameters were as follows: sweep rate, 100 mV s^{-1}; solvent, 30% aqueous DMF with 0.1 M Et_4NClO_4.

The effect of the N4 substituent on the $Fe^{III/II}$ redox potential was the same in each of the three series $(Fe(DpT)_2$, $Fe(BpT)_2$, and $Fe(NBpT)_2)$. That is, the complexes with a −NHPh terminal

group show by far the highest redox potentials, while the remaining complexes cluster around a similar potential.

Biological Studies. Antiproliferative Activity against Tumor Cells: BpT and NBpT Ligands. The ability of the BpT and NBpT series to inhibit cellular proliferation was assessed using SK-N-MC neuroepithelioma cells, as the effect of Fe chelators on their growth has been well characterized.[17,41,48−50] These novel ligands were compared to their parent compounds, the DpT series, and a number of relevant positive controls. These included DFO, which is used for the treatment of Fe overload, the well-described ligand NIH (Figure 1A),[49,50] and the clinically trialed chelator 3-AP that has been designed for cancer therapy.[10,51] These results are presented in Table 2.

This study identified both the BpT and NBpT analogues as having high antiproliferative activity (Table 2). In particular, the chelators Bp4mT, Bp44mT, Bp4eT, Bp4aT, and Bp4pT demonstrated potent antiproliferative effects (IC_{50} = 0.002−0.005 μM; Table 2). This identifies the BpT analogues as the most effective series of chelators with antiproliferative activity ever developed within our laboratory. All members of the BpT and NBpT series, excluding BpT, NBpT, and NBp44mT, demonstrated significantly ($p < 0.05$) greater efficacy than the controls DFO (IC_{50} = 4.51 μM; Table 2), NIH (IC_{50} = 0.71 μM; Table 2), and 3-AP (IC_{50} = 0.26 μM; Table 2). In addition, the majority of the BpT and NBpT series demonstrated significantly ($p < 0.05$) greater antiproliferative effects than their corresponding DpT parent chelators. While BpT and NBpT showed efficacy comparable to that of DpT, only Bp44mT, NBp44mT, and NBp4pT exhibited significantly ($p < 0.05$) less antiproliferative activity than their pyridyl analogues Dp44mT and Dp4pT. The particularly low antiproliferative effects of NBp44mT (IC_{50} = 1.61 μM), in comparison to its BpT and DpT analogues, can be attributed to its instability in aqueous solution, as described previously (see Characterization of the Free Ligands). The more hydrophilic chelators BpT (IC_{50} = 4.66 μM; Table 2) and NBpT (IC_{50} = 3.82 μM, Table 2) demonstrated the lowest antiproliferative activity.

Fe Complexes of BpT and NBpT. Previous studies have illustrated that complexation of aroylhydrazone chelators with metals can result in marked changes in their biological activity.[49,52−54] To determine the effect of complexation on the antiproliferative behavior of the BpT and NBpT series, their Fe^{II} and Fe^{III} complexes were synthesized and their antiproliferative activity was examined using SK-N-MC neuroepithelioma cells. In comparison with their free ligands, the Fe^{II} and Fe^{III} complexes of all members of the BpT and NBpT series, excluding BpT and NBpT, demonstrated significantly ($p < 0.005$) decreased antiproliferative activity (Table 2). In fact, complexation resulted in a 2- to 200-fold increase of the IC_{50} value.

Both the Fe^{II} and Fe^{III} complexes of BpT resulted in significantly ($p < 0.05$) enhanced antitumor activity (Table 2) when compared to the free ligand, decreasing the IC_{50} value by a factor of 4. However, this should be viewed in perspective, as both the BpT free ligand and its Fe complexes were much less cytotoxic than the other analogues from this series (IC_{50} values more than 2 orders of magnitude higher). Several properties have been suggested to explain the increased antiproliferative activity of the Fe complexes in comparison to the free ligands.[52] First, the formation of the Fe complex may result in a more lipophilic species because of the inaccessibility of the donor atoms to the solvent, which is better able to penetrate cellular membranes in comparison to the free ligand.[52] Hence, precomplexation may lead to higher concentrations of the redox-active Fe complexes within cells, resulting in greater antiproliferative effects.[16,27,52,55] Second, lipophilic metal complexes may act as transport vehicles, dissociating after entry and as a consequence donating the toxic metal ion to the cell, acting as lipid soluble delivery shuttles.[56,57] Considering that BpT was found to be one of the most hydrophilic members of the BpT series, its Fe complex may act as a lipophilic shuttle, allowing intracellular access of the ligand and metal, mediating their cytotoxic effects simultaneously.

Table 3. IC_{50} (μM) Values of Bp4mT, Bp44mT, Bp4eT, Bp4aT, Bp4pT, NBp4eT, and NBp4aT at Inhibiting the Growth of Mortal MRC-5 Fibroblasts in Comparison to SK-N-MC Neuroepithelioma Cells As Determined by the MTT Assay[a]

	IC_{50} (μM)		
chelator	MRC-5 fibroblasts	SK-N-MC neuroepithelioma	*p*
Bp4mT	>6.25	0.004 ± 0.002	<0.001
Bp44mT	>6.25	0.004 ± 0.001	<0.001
Bp4eT	>6.25	0.002 ± 0.001	<0.001
Bp4aT	>6.25	0.004 ± 0.003	<0.001
Bp4pT	1.86 ± 1.77	0.005 ± 0.002	>0.05
NBp4eT	2.31 ± 0.25	0.014 ± 0.004	<0.001
NBp4aT	2.39 ± 0.35	0.013 ± 0.001	<0.001

[a] Cells were seeded and allowed to attach to wells for 24 h and then incubated for 72 h at 37 °C with control medium or the chelators. Results are the mean ± SD (three experiments). The *p* values were determined using Student's *t*-test and were used to compare the activity of the ligand in normal and neoplastic cells. A value of $p < 0.05$ was considered as significant.

Antiproliferative Activity against Normal Cells. For an Fe chelator to be considered as an antitumor agent, it must exhibit potent antiproliferative activity against neoplastic cells while leaving normal cells unaffected. A selection of the most potent cytotoxic analogues, namely, Bp4mT, Bp44mT, Bp4eT, Bp4aT, Bp4pT, NBp4eT, and NBp4aT, were examined for their effect on the proliferation of mortal MRC-5 fibroblasts (Table 3). It is immediately apparent that when SK-N-MC neuroepithelioma cells and MRC-5 fibroblasts were compared, there was a marked and significant ($p < 0.001$) difference (more than 3 orders of magnitude) in IC_{50} values of all tested analogues except Bp4pT. This suggested an appreciable therapeutic index in targeting cancer cells over normal cells.

Cellular Fe Efflux. In an effort to understand the mechanisms of action of the BpT and NBpT series, initial experiments characterized the ability of these chelators to mobilize intracellular ^{59}Fe from prelabeled SK-N-MC neuroepithelioma cells (Figure 4A). The release of ^{59}Fe mediated by these ligands was compared to that of their parent compounds, the DpT series, as well as a number of positive controls, including DFO, NIH, and PIH (Figure 1A), which have been characterized in detail.[10,41,50]

Both NIH and PIH showed high ^{59}Fe mobilization activity, releasing 45 ± 4% and 47 ± 3% of intracellular ^{59}Fe, respectively, as shown previously.[49,50,58] In comparison, the control, which was culture media alone, mediated 4 ± 1% of intracellular ^{59}Fe release. The clinically used chelator, DFO, demonstrated poor ^{59}Fe mobilization efficacy, resulting in the release of only 7 ± 1% of intracellular ^{59}Fe (Figure 4A).

All members of the BpT and NBpT series led to ^{59}Fe mobilization activity, resulting in the release of 23−41% and 19−43% of cellular ^{59}Fe, respectively. Considering the BpT and NBpT series of ligands, Bp4eT and NBpT showed the greatest Fe chelation efficacy (Figure 4A). The chelators NBpT, NBp4mT, NBp4aT, Bp44mT, and Bp4eT demonstrated ^{59}Fe mobilization activity comparable to that of PIH and NIH. In

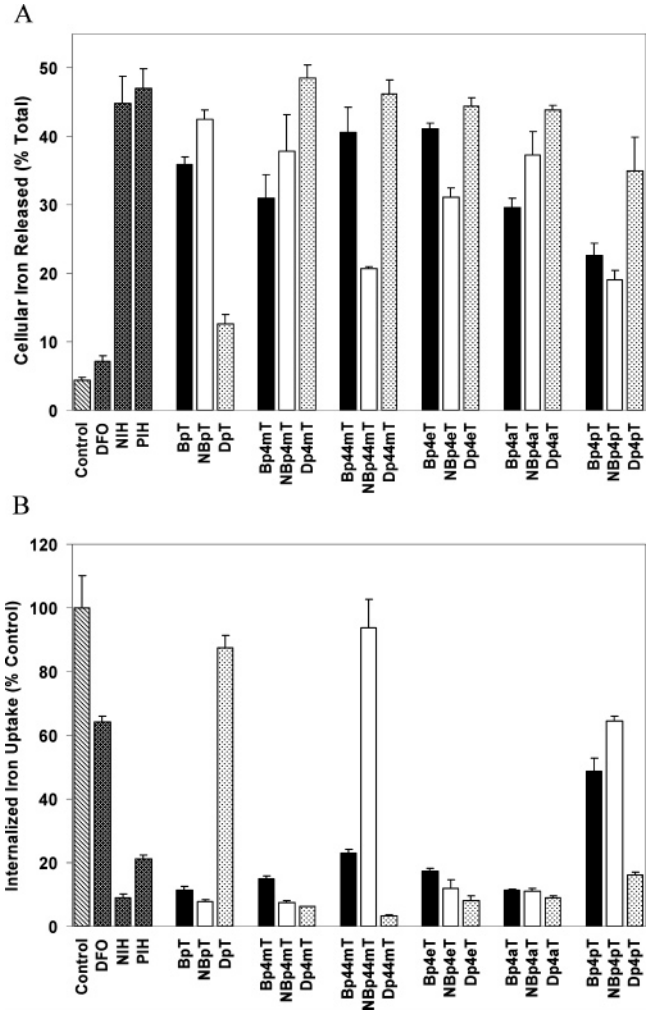

Figure 4. Effect of the DpT, BpT, and NBpT series chelators on (A) ^{59}Fe mobilization from prelabeled SK-N-MC neuroepithelioma cells and (B) ^{59}Fe uptake from ^{59}Fe transferrin (^{59}Fe-Tf) by SK-N-MC neuroepithelioma cells. Results are the mean ± SD of three experiments with three determinations in each experiment.

contrast, all other members of the BpT and NBpT series were significantly ($p < 0.05$) less active. All the BpT and NBpT analogues were significantly ($p < 0.001$) more effective than DFO. The chelator-mediated increase in cellular Fe mobilization was not mediated by their cytotoxic effects as the cells remained viable within the short 3 h of incubation used.

Comparison of the BpT and NBpT series to their parent DpT analogues revealed that only BpT and NBpT were significantly ($p < 0.0005$) more active than their analogous 2-pyridyl-substituted chelator, DpT, mediating 36 ± 1% and 43 ± 1% of ^{59}Fe release, respectively (Figure 4A). DpT has previously been shown to be the most hydrophilic and least active chelator of the DpT series,[29] suggesting that its hydrophilic nature limits membrane permeability. The higher lipophilicity of BpT and NBpT in comparison with that of DpT (Table 2) probably promotes membrane permeability leading to increased ^{59}Fe efflux (Figure 4A). While Bp44mT showed efficacy comparable to that of Dp44mT, all other members of the BpT and NBpT series were less active than their corresponding DpT chelators. This was most marked when comparing Bp4pT and NBp4pT to Dp4pT.

No clear trends were evident upon comparison of the ^{59}Fe mobilization activity of the BpT series against their NBpT counterparts.

Inhibition of Cellular ^{59}Fe Uptake from ^{59}Fe Transferrin. The ability of the BpT and NBpT series chelators to inhibit ^{59}Fe uptake from the serum Fe-binding protein Tf in SK-N-MC neuroepithelioma cells was also assessed. This is important, as inducing Fe deprivation and antiproliferative activity involves both increasing Fe mobilization and preventing Fe uptake from Tf. As demonstrated in our previous work,[10,50,58] the positive controls NIH and PIH were found to effectively reduce ^{59}Fe uptake to 9 ± 1% and 21 ± 1% of the control, respectively (Figure 4B). In contrast, the hydrophilic chelator, DFO, exhibited poor ability to decrease ^{59}Fe uptake to only 64 ± 2% of the control (Figure 4B), as shown previously.[50,58]

With the exception of Bp4pT, NBp44mT, and NBp4pT, all members of the BpT and NBpT series markedly reduced ^{59}Fe uptake to between 11−17% and 7−12% of the control, respectively (Figure 4B). The chelators of the BpT and NBpT series that were most effective at reducing ^{59}Fe uptake from ^{59}Fe-Tf included NBpT, NBp4mT, and NBp4aT that reduced this to 7 ± 1%, 8 ± 1%, and 11 ± 1% of the control, respectively. On the other hand, NBp44mT demonstrated efficacy comparable to that of the control medium. This is most likely caused by the hydrolysis of the ligand in aqueous solution, as described previously. The lack of activity of Bp4pT and NBp4pT may be due to their high lipophilicity. In this case, compounds that are too lipophilic may result in retention in cellular membranes, leading to reduced Fe chelation efficacy. Similar results have been observed for other highly lipid soluble Fe chelators.[59]

Interestingly, those members of the BpT and NBpT series that exhibited high ^{59}Fe mobilization activity also demonstrated increased efficacy to prevent ^{59}Fe uptake from ^{59}Fe-Tf. In fact, plotting the efficacy of the chelator to reduce internalized ^{59}Fe uptake against their ability to mediate ^{59}Fe mobilization led to a linear relationship ($r = -0.90$) for the NBpT series, while a weaker relationship ($r = -0.44$) was observed for the BpT analogues.

Excluding BpT, most of the BpT series were significantly ($p < 0.05$) less effective than NIH at inhibiting ^{59}Fe uptake from ^{59}Fe-Tf. In contrast, all members of the NBpT series except NBp44mT and NBp4pT demonstrated Fe chelation efficacy comparable to that of NIH. Besides NBp44mT, Bp4pT, and NBp4pT, all analogues of the BpT and NBpT series displayed significantly ($p < 0.05$) greater ability than PIH to inhibit ^{59}Fe uptake. DFO demonstrated significantly ($p < 0.005$) less ability to prevent ^{59}Fe uptake from ^{59}Fe-Tf than the majority of the BpT and NBpT series, while NBp4pT demonstrated efficacy comparable to that of DFO. In contrast, DFO was significantly ($p < 0.005$) more active than NBp44mT at preventing ^{59}Fe uptake from ^{59}Fe-Tf.

Apart from DpT itself, most of the DpT parent chelators were found to be significantly ($p < 0.05$) more effective at preventing ^{59}Fe uptake than their corresponding BpT and NBpT analogues.

Most of the NBpT analogues, except NBp4pT and NBp44mT, were significantly ($p < 0.05$) more effective at inhibiting ^{59}Fe uptake from ^{59}Fe-Tf than their BpT counterparts. These results suggest that an optimal log *P* value exists and that NBp4pT is too hydrophobic and suffers from poor bioavailability. It is noted that despite their high activity in both ^{59}Fe efflux and uptake studies (Figure 4), the antiproliferative activity of the BpT and NBpT ligands was poor (Table 2).

Relationship between Antiproliferative Activity and the Chemical and Biological Properties of the Chelators. Regression analyses comparing the ^{59}Fe efflux and antiproliferative activity of the BpT and NBpT series were examined to

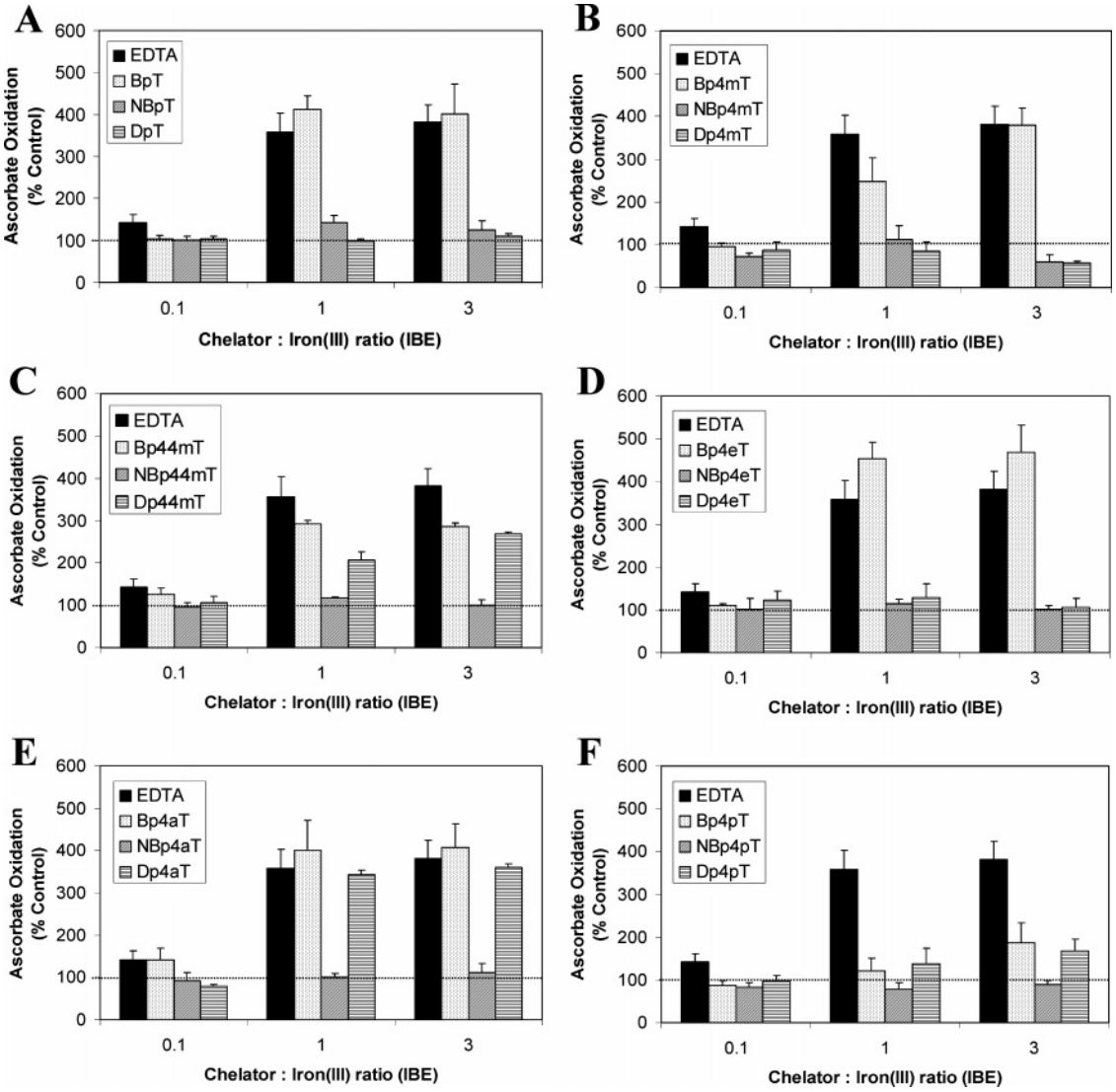

Figure 5. Effect of the Fe complexes of the BpT, NBpT, and DpT series on ascorbate oxidation. Chelators at iron-binding equivalent (IBE) ratios of 0.1, 1, and 3 were incubated in the presence of Fe^{III} (10 μM) and ascorbate (100 μM). The UV−vis absorbance at 265 nm was recorded after 10 and 40 min, and the difference between the time points was calculated. Shown are comparisons of EDTA with (A) BpT, NBpT, and DpT; (B) Bp4mT, NBp4mT, and Dp4mT; (C) Bp44mT, NBp44mT, and Dp44mT; (D) Bp4eT, NBp4eT, and Dp4eT; (E) Bp4aT, NBp4aT, and Dp4aT; and (F) Bp4pT, NBp4pT, and Dp4pT. Results are the mean ± SD (three experiments).

determine if a relationship existed between these factors (data not shown). The chelators BpT and NBpT were excluded because of their very low antiproliferative effects (Table 2). A linear relationship was observed between ^{59}Fe efflux and antiproliferative activity of the BpT series ($r = -0.77$), while a weaker relationship was evident with the NBpT analogues ($r = -0.50$). This suggested that the Fe mobilization efficacy of the BpT series may play an important role in their antiproliferative activity.

Plots comparing the ability of the ligands to reduce ^{59}Fe uptake and induce antiproliferative activity were also analyzed, again excluding BpT and NBpT. These data illustrated a linear relationship within the BpT series ($r = 0.57$), while no clear relationship was found between inhibiting Fe uptake and preventing proliferation for the NBpT series.

Analysis of the relationship between measured redox potentials and antiproliferative activity determined that a linear relationship existed for the BpT series ($r = 0.74$), while no clear relationship was evident between these factors for the NBpT series ($r = -0.17$). These results indicated that no single factor was responsible for the observed cytotoxicity. Rather, a combination of properties including lipophilicity, ^{59}Fe mobilization activity, the ability to inhibit ^{59}Fe uptake from Tf, and redox-cycling result in the antiproliferative effects of these chelators.

Ascorbate Oxidation by the BpT and NBpT Fe Complexes. The electrochemical studies reported in Table 2 illustrate the facile interconversion between the ferric and ferrous states at potentials accessible to biological oxidants and reductants. Hence, the ability of the BpT and NBpT series to catalyze the oxidation of a physiological substrate was important to determine if redox activity played a role in antiproliferative activity. Thus, the oxidation of ascorbate mediated by the Fe complexes of the BpT and NBpT series was examined in comparison to their parent chelators, the DpT analogues (Figure 5). EDTA was also included as a positive control because its activity in this assay has been well characterized.[27,55,60]

In all experiments examining the redox properties of chelators, results were expressed as iron-binding equivalents (IBE). This was due to the different coordination modes of the ligands to Fe; i.e., EDTA is hexadentate and forms 1:1 ligand/Fe complexes, while the DpT, BpT, and NBpT analogues are tridentate

resulting in 2:1 complexes.[29,60] In the present study, a range of ligand/Fe IBE ratios were used, namely, 0.1, 1, and 3. An IBE of 0.1 represents an excess of Fe to chelator, i.e., 1 hexadentate chelator or 2 tridentate chelators in the presence of 10 Fe atoms. An IBE of 1 is equivalent to the complete filling of the coordination sphere, i.e., 1:1 Fe/EDTA or 1:2 Fe/DpT. An IBE of 3 represents an excess of chelator to Fe and is equal to either 3 hexadentate or 6 tridentate ligands in the presence of 1 Fe atom.[29,60]

The positive control, EDTA, increased ascorbate oxidation to 357% and 382% of the control at an IBE of 1 and 3, respectively, while showing little activity at an IBE of 0.1 (Figure 5). This is in agreement with previous studies demonstrating the ability of the EDTA/Fe complex to undergo facile redox cycling and catalyze ascorbate oxidation.[16,27,29,55,60,61]

Marked differences in the ability of the BpT and NBpT series to catalyze Fe^{III}-mediated ascorbate oxidation were evident (Figure 5). Excluding Bp4pT, the BpT analogues markedly increased ascorbate oxidation to 249−454% and 287−469% of the control at an IBE of 1 and 3, respectively. Bp4pT was the only BpT analogue to demonstrate poor activity, mediating only 121% and 186% ascorbate oxidation of the control at an IBE of 1 and 3 (Figure 5F). When compared to their analogous DpT chelators at IBEs of 1 and 3, the BpT ligands were found to be significantly ($p < 0.05$) more effective at oxidizing ascorbate. The only exceptions to this were Bp4aT and Bp4pT, which were comparable to Dp4aT (Figure 5E) and Dp4pT (Figure 5F) respectively. While the chelators BpT, Bp4mT, and Bp4aT showed ascorbate oxidation activity comparable to that of EDTA, Bp4eT was the only analogue to exhibit significantly ($p < 0.01$) higher ascorbate oxidative activity than EDTA at an IBE of 1 and 3. These data may explain the increased antiproliferative activity of Bp4eT ($IC_{50} = 0.002$ μM; Table 2), which showed the greatest antitumor effects of the BpT and NBpT series. This result was also in good agreement with electrochemistry studies, which demonstrated that the Bp4eT Fe complex (+99 mV, Table 2) exhibited the lowest redox potential of the BpT series, enabling facile interconversion between the ferric and ferrous states to generate ROS.

Chelators possessing the 4-phenyl moiety such as Dp4pT, Bp4pT, and NBp4pT demonstrated the least ascorbate oxidation activity (Figure 5F). This could be related to the fact these ligands exhibited among the highest redox potentials (+180 to 249 mV, Table 2) that would retard redox cycling between the Fe^{II} and Fe^{III} states and prevent ascorbate oxidation.

The majority of the NBpT series showed significantly ($p < 0.05$) reduced ability to mediate ascorbate oxidation compared with their BpT counterparts, ranging between 79−143% and 60−124% of the control at IBEs of 1 and 3, respectively (Figure 5). In comparison to EDTA, all members of the NBpT series were significantly ($p < 0.005$) less effective at inducing ascorbate oxidation at IBEs of 0.1, 1, and 3. The NBpT series generally demonstrated comparable capacity to catalyze the oxidation of ascorbate as the DpT analogues at all IBEs. This indicated that the increased cytotoxic effects of some NBpT series chelators in comparison to their DpT counterparts was not due to differences in redox cycling. Indeed, other factors such as lipophilicity may dictate their increased antiproliferative effects.

For catalytic ascorbate oxidation to be mediated effectively by an Fe complex, the Fe^{II} complex (formed by reduction of the Fe^{III} precursor) must be able to be reoxidized by dioxygen. In other words, a high redox potential will inhibit the oxidative half reaction while a low redox potential will retard the reductive half reaction. Plots analyzing the relationship between ascorbate oxidation activity and redox potential of the BpT series showed a linear relationship at an IBE of 1 ($r = -0.90$) and 3 ($r = -0.89$). This suggested that the oxidative half reaction is rate-limiting in this process.

In summary, the results of this ascorbate oxidation study imply that while redox activity plays an important role in the antiproliferative effects of the NBpT and DpT series, their redox activity was not nearly as extensive as the BpT series. This further emphasizes that the higher antiproliferative activity of the BpT series is due, at least in part, to their profound redox activity that can induce oxidative damage.

Benzoate Hydroxylation. As a further assessment of redox activity of the Fe complexes, it was of interest to examine benzoate hydroxylation in the presence of Fe^{III} and the ligand (Figure 6). These experiments gauge the ability of an Fe complex to catalyze the breakdown of hydrogen peroxide to generate hydroxyl radicals via so-called Fenton chemistry leading to benzoate hydroxylation.[60]

The Fe^{III} complex of EDTA (the positive control) increased benzoate hydroxylation to 218% and 281% at IBEs of 1 and 3, respectively (Figure 6). This effect was in agreement with previous studies.[60] Consistent with the ascorbate oxidation results, all the BpT analogues except Bp4pT significantly ($p < 0.05$) increased benzoate hydroxylation, especially at an IBE of 3. The greatest hydroxylation of benzoate was observed with BpT, while Bp44mT, Bp4aT, Bp4eT, and Bp4mT had intermediate ability, increasing benzoate hydroxylation to 151%, 159%, 170%, and 197% of the control, respectively, at an IBE of 3 (Figure 6). Bp4pT showed the least benzoate hydroxylation activity, being similar to the control at an IBE of 3 (Figure 6F).

In contrast to the BpT series, all the NBpT analogues except NBpT had little effect on benzoate hydroxylation compared to the control (Figure 6). Again, the strong electron-withdrawing effects of the nitro substituent and the resultant high redox potentials (Table 2) may be responsible for this latter effect and the marked reduction in redox activity of the NBpT analogues. The DpT series also increased benzoate hydroxylation in the presence of Fe^{III}, although to a lesser extent than the BpT analogues (Figure 6). Furthermore, as observed for the BpT series, the phenyl substituted analogue Dp4pT resulted in the least benzoate hydroxylation.

Conclusions

The work performed in this study highlights several important structure−activity relationships critical for the design of potent and selective Fe chelators for the treatment of cancer. The increased antineoplastic activity of the BpT series can be attributed, at least in part, to the lower redox potentials of their Fe complexes than their corresponding DpT and NBpT Fe complexes. In fact, the unsubstituted phenyl moiety of the BpT series may contribute toward the lowered $Fe^{III/II}$ redox potentials of the BpT Fe complexes, leading to higher redox activity. This was supported by ascorbate oxidation and benzoate hydroxylation studies that demonstrated that the Fe^{III}-BpT complexes were able to redox-cycle and stimulate redox reactions to a greater degree than the DpT and NBpT Fe complexes. Thus, the 2-benzoylpyridine moiety was found to be an important structural characteristic necessary for potent antiproliferative activity.

The incorporation of an electron-withdrawing group (i.e., $-NO_2$) increased the redox potential of the NBpT series Fe complexes. This was detrimental to the redox activity of the complex and was in agreement with previous studies using other

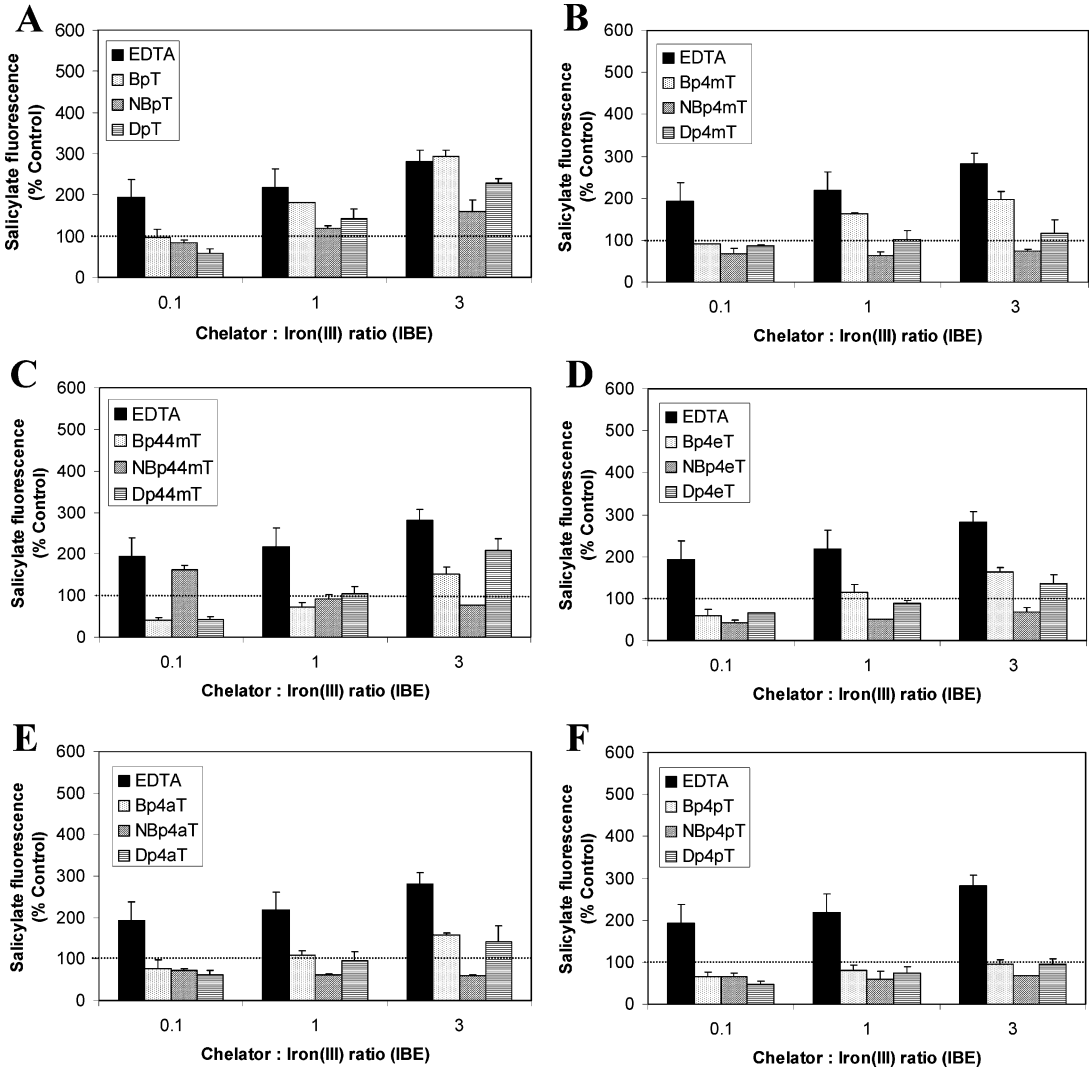

Figure 6. Effect of various Fe chelators on the hydroxylation of benzoate in the presence of Fe^{III} and hydrogen peroxide. Chelators at iron-binding equivalent (IBE) ratios of 0.1, 1, and 3 were incubated for 1 h at room temperature in the presence of Fe^{III} (30 μM), hydrogen peroxide (5 mM), and benzoate (1 mM). The fluorescence of hydroxylated benzoate was measured at 308 nm excitation and 410 nm emission. Shown are comparisons of EDTA with (A) BpT, NBpT, and DpT; (B) Bp4mT, NBp4mT, and Dp4mT; (C) Bp44mT, NBp44mT, and Dp44mT; (D) Bp4eT, NBp4eT, and Dp4eT; (E) Bp4aT, NBp4aT, and Dp4aT; and (F) Bp4pT, NBp4pT, and Dp4pT. Results are the mean ± SD (three experiments).

Fe chelators, which identified that electron-withdrawing substituents increased redox potentials.[62−64] Clearly, the introduction of the nitrophenyl group in the NBpT series of chelators was unfavorable to their antiproliferative efficacy and strongly suggests that the addition of electron-donating substituents to this class of chelators is crucial to their future design. On the other hand, the nitrophenyl group enabled facile crystallization of the ligand and its Fe complex, which was not easily achieved in its absence.

Collectively, the current results demonstrate that the potent and selective antiproliferative activity of the BpT series against tumor cells was due, at least in part, to their enhanced redox activity. However, while redox activity plays a role in their antiproliferative efficacy, combinations of properties including lipophilicity, ^{59}Fe mobilization activity, and the ability to inhibit ^{59}Fe uptake from Tf are also critical factors.

Experimental Section

Chemistry Studies. Syntheses. 2-(3′-Nitrobenzoyl)pyridine was synthesized by a standard procedure.[65] All other reagents were obtained commercially and used without further purification. Desferrioxamine (DFO) was obtained from Novartis (Basel, Switzerland). 3-AP (Triapine) was a gift from Vion Pharmaceuticals, New Haven, CT.

Physical Methods. NMR spectra were measured at 400 MHz on a Bruker instrument. IR spectra were obtained on a Perkin-Elmer 1600 series spectrophotometer using an ATR (attenuated total reflectance) assembly. Cyclic voltammetry was performed with a BAS100B/W potentiostat. A glassy carbon working electrode, an aqueous Ag/AgCl reference electrode, and a Pt wire auxiliary electrode were used. All complexes were at ∼1 mM concentration in DMF/H_2O, 70:30 v/v. The supporting electrolyte was Et_4NClO_4 (0.1 M), and the solutions were purged with nitrogen prior to measurement. All potentials are cited versus the normal hydrogen electrode (NHE) by addition of 196 mV to the potentials measured relative to the Ag/AgCl reference.

Elemental analysis (C, H, N, S) of the ligands and complexes was performed, and the results, available as Supporting Information, were within ±0.4% of the theoretical values, unless otherwise stated.

Crystallography. Cell constants at 293 K were determined by a least-squares fit to the setting parameters of 11 independent reflections measured on an Enraf-Nonius CAD4 four-circle diffractometer employing graphite-monochromated Mo Kα radiation (0.710 73 Å) and operating in the $\omega-2\theta$ scan mode within the range $2 < 2\theta < 50$ Å. Data reduction and analytical absorption corrections were performed as described.[66] Structures were solved by direct

methods and refined by full-matrix least-squares analysis with RAELS.[67] All non-H atoms were refined with anisotropic thermal parameters. H-atoms were included at estimated positions using a riding model. Molecular structure diagrams were produced with ORTEP-II.[68]

General Synthesis of BpT Analogues. 2-Benzoylpyridine (1.934 g, 10 mmol) was dissolved in EtOH (15 mL), and a solution of 10 mmol of the appropriate thiosemicarbazide in water (15 mL) was added. Glacial acetic acid (5−6 drops) was added, and the mixture was gently refluxed for 4−5 h. The mixture was allowed to cool to room temperature and kept at 4 °C overnight to complete precipitation. The yellow product was filtered off and washed with EtOH and diethyl ether.

Bp4mT (from 4-Methylthiosemicarbazide). Yield 92%. Anal. Calcd for $C_{14}H_{14}N_4S$: C, 61.2; H, 5.3; N, 20.4; S, 11.7%. Found: C, 61.1; H, 5.1; N, 20.5; S, 12.3%. IR (cm^{-1}) 3296m, 1530s, 1468s, 1308m, 1224s, 1107s, 1042m, 998m, 816m, 797s, 767m, 730m, 694s, 644s, 598m. ^{1}H NMR (DMSO-d_6): δ 8.85 (d, 1H, pyr), 8.71 (d, 1H, pyr), 8.01 (t, 1H, pyr), 7.63 (m, 3H, $-C_6H_5$ or pyr), 7.45 (m, 3H, pyr or $-C_6H_5$), 7.31 (m, 1H, pyr or $-C_6H_5$), 3.04 (d, 3H, $-CH_3$).

Bp44mT (from 4,4-Dimethylthiosemicarbazide). Yield 86%. Anal. Calcd for $C_{15}H_{16}N_4S$: C, 63.4; H, 5.7; N, 19.7; S, 11.3%. Found: C, 62.8; H, 5.9; N, 19.5; S, 10.6%. IR (cm^{-1}) 2871w, 1571m, 1493m, 1461w, 1424w, 1368m, 1339m, 1305s, 1268w, 1234s, 1159s, 1117s, 1062m, 1002s, 961s, 902s, 788s, 720s, 698s, 656w, 645w. ^{1}H NMR (DMSO-d_6): δ 8.70 (dd, 1H), 8.45 (dd, 1H), 8.12−7.84 (dd, 2H), 7.66−7.44 (dd, 4H), 7.33 (dt, 1H), 3.35 (s, 3H), 3.25 (s, 3H).

Bp4eT (from 4-Ethylthiosemicarbazide). Yield 91%. Anal. Calcd for $C_{15}H_{16}N_4S$: C, 63.4; H, 5.7; N, 19.7; S, 11.3%. Found: C, 62.9; H, 5.5; N, 19.5; S, 11.2%. IR (cm^{-1}) 3290w, 1583m, 1529s, 1434s, 1416m, 1371w, 1304s, 1251m, 1208s, 1152w, 1089s, 1050s, 997w, 935m, 923m, 890w, 813s, 793s, 762w, 728s, 699s, 644s, 601w. ^{1}H NMR (DMSO-d_6): δ 8.75 (t, 1H), 8.03 (td, 1H), 7.63−7.56 (td, 1H), 7.47−7.42 (m, 3H), 7.34 (dt, 1H), 3.65 (m, 2H), 1.16 (t, 3H).

Bp4aT (from 4-Allylthiosemicarbazide). Yield 80%. Anal. Calcd for $C_{16}H_{16}N_4S$: C, 64.8; H, 5.4; N, 18.9; S, 10.8%. Found: C, 64.7; H, 5.5; N, 19.5; S, 10.6%. IR: (cm^{-1}) 3370w, 1642w, 1582w, 1516s, 1468w, 1442w, 1422w, 1300w, 1247m, 1205m, 1179m, 1150w, 1114m, 1072w, 1047w, 991w, 962w, 921s, 836m, 796s, 770s, 734m, 699s, 664m, 619s, 567m. ^{1}H NMR (DMSO-d_6): δ 8.03 (d, 1H), 8.00 (d, 4H), 7.98 (d, 2H), 7.64−7.55 (m, 4H), 7.47−7.44 (d, 4H), 7.35 (q, 1H), 5.94 (m, 1H), 5.1 (dd, 1H), 4.23 (t, 2H).

Bp4pT (from 4-Phenylthiosemicarbazide). Yield 84%. Anal. Calcd for $C_{19}H_{16}N_4S$ C: 68.7; H, 4.9; N, 16.9; S, 9.6%. Found: C, 68.0; H, 4.8; N, 16.8; S, 9.6%. IR (cm^{-1}) 3299w, 3051w, 1592s, 1528s, 1466w, 1438m, 1366w, 1302m, 1252w, 1202w, 1171m, 1104s, 1027w, 998w, 920w, 835w, 785m, 755s, 730m, 691s, 634s, 591w. ^{1}H NMR (DMSO-d_6): δ 10.67(s, 1H), 10.30 (s, 1H), 8.88 (d, 3H), 7.72−7.71 (td, 3H), 7.61−7.55 (dq, 4H), 7.54−7.40 (td, 2H), 7.23 (tt, 2H).

BpT (from Thiosemicarbazide). Yield 90%. Anal. Calcd for $C_{13}H_{12}N_4S$: C, 60.9; H, 4.7; N, 21.9; S, 12.51%. Found: C, 60.3; H, 4.6; N, 21.7; S, 12.2%. IR: (cm^{-1}) 3220w, 1590s, 1453m, 1417s, 1326m, 1273w, 1253w, 1103w, 1088w, 1072w, 1048m, 1024w, 998w, 971w, 943w, 921w, 844s, 797s, 769s, 703s, 652s, 630m, 605m. ^{1}H NMR (DMSO-d_6): δ 8.79 (dq, 1H), 8.85 (dq, 1H), 8.59 (s, 1H), 8.05 (dd, 1H), 7.97−7.54 (m, 3H), 7.45−7.33 (dt, 3H).

General Synthesis of NBpT Analogues (except NBp44mT). 2-(3′-Nitrobenzoyl)pyridine (2.18 g, 9.5 mmol) was dissolved in 15 mL of absolute ethanol, and 9.5 mmol of the appropriate thiosemicarbazide was directly added as a solid. Concentrated HCl (5−6 drops) was added, and the mixture was gently refluxed for 4−6 h. The mixture was allowed to cool to complete precipitation. The yellow product was collected by vacuum filtration and washed with ethanol and then diethyl ether.

NBp4mT. Yield 65%. Anal. Calcd for $C_{14}H_{13}N_5O_2S$: C, 49.1; H, 4.7; N, 20.5; S, 9.4%. Found: C, 49.4; H, 4.0; N, 20.5; S, 9.5. IR (cm^{-1}) 3082w, 1610s, 1561s, 1520s, 1475s, 1451s, 1347s, 1323w, 1300w, 1210s, 1159w, 1130m, 1095w, 1053s, 1003m, 947w, 889w, 825s, 774s, 758s, 739w, 691s, 652w, 623w, 611m. ^{1}H NMR (DMSO-d_6): δ 8.89 (t, 1H, pyr), 8.42 (t, 3H, pyr), 8.10 (t, 1H, pyr), 8.02 (d, 1H, $-C_6H_5$ or pyr), 7.87 (d, 3H, pyr or $-C_6H_5$), 7.74 (s, 1H, pyr), 7.43 (t, 1H, pyr), 3.05 (t, 3H, $-CH_3$).

NBp4eT. Yield 63%. Anal. Calcd for $C_{15}H_{15}N_5O_2S$: C, 49.3; H, 5.2; N, 19.2; S, 8.8%. Found: C, 49.1; H, 4.3; N, 19.0; S, 8.7%. IR (cm^{-1}) 3079w, 1607m, 1525s, 1479s, 1447s, 1350s, 1294m, 1198s, 1161w, 1129w, 1091m, 1055w, 996m, 962w, 942w, 915w, 885w, 819w, 790w, 776s, 736s, 693s, 651w, 618s, 608s. ^{1}H NMR (DMSO-d_6): δ 8.88 (t, 1H), 8.44 (td, 1H), 8.04 (d 1H), 7.95−7.88 (d, 3H), 7.77−7.55 (t, 2H), 7.43(dt, 1H), 3.66 (m, 2H), 1.16 (t, 3H).

NBp4aT. Yield 63%. Anal. Calcd for $C_{15}H_{15}N_5O_2S$: C, 52.2; H, 4.9; N, 19.0; S, 8.7. Found: C, 52.1; H, 4.3; N, 19.0; S, 8.7. IR (cm^{-1}) 3129w, 1607m, 1517s, 1473s, 1451m, 1346s, 1299w, 1275w, 1234w, 1182s, 1122s, 1096s, 1038w, 998s, 939s, 916m, 884w, 845w, 826w, 814w, 778s, 734s, 694s, 665m, 643m, 621m. ^{1}H NMR (DMSO-d_6): δ 9.06 (t, 1H, pyr), 8.89 (t,1H, pyr), 8.84 (d, 1H, pyr), 8.43−8.28 (dt, 5H, pyr), 8.15−8.03 (d, 2H, pyr), 7.90−7.86 (dd, 3H), 7.77−7.62 (m, 3H), 7.44 (d, 1H, pyr), 5.94 (m, 2H), 5.1 (dd, 2H), 4.23 (t, 1H).

NBp4pT. Yield 69%. Anal. Calcd for $C_{19}H_{15}N_5O_2S$: C, 55.2; H, 4.6; N, 16.9; S, 7.8%. Found: C, 54.9; H, 3.9; N, 17.0; S, 7.7%. IR (cm^{-1}) 3076w, 1607m, 1523s, 1482s, 1442s, 1348s, 1317m, 1231m, 1182s, 1158s, 1035w, 998m, 937m, 816w, 778s, 740s, 695s, 659w, 605s. ^{1}H NMR (DMSO-d_6): δ 10.90 (s, 1H), 10.48 (s, 1H), 8.90 (d, 3H), 8.46−8.07 (td, 5H), 7.96 (t, 1H),7.61−7.55 (dq, 4H), 7.54−7.40 (td, 2H), 7.20 (tt, 2H).

NBpT. Yield 66%. Anal. Calcd for $C_{13}H_{11}N_5O_2S$: C, 46.9; H, 4.4; N, 21.0; S, 9.6%. Found: C, 46.2; H, 3.4; N, 20.5; S, 9.5%. IR (cm^{-1}) 3074m, 1635w, 1613s, 1561m, 1524s, 1481s, 1449s, 1350s, 1300m, 1254s, 1227m, 1204m, 1160w, 1132w, 1094m, 1065m, 1041w, 1004w, 970w, 911m, 886s, 843s, 781s, 765s, 729s, 695s, 644s, 603s. ^{1}H NMR (DMSO-d_6): δ 8.90 (dq, 1H), 8.85 (dq, 1H), 8.59 (s, 1H, −N4), 8.05 (dd, 1H), 7.97−7.54 (m, 3H), 7.45−7.33 (dt, 3H).

NBp44mT. 2-(3′-Nitrobenzoyl)pyridine (0.10 g) was dissolved in 10 mL of acetonitrile, and 0.09 g of 4,4-dimethyl thiosemicarbazide was directly added as a solid with stirring. Glacial acetic acid (5−6 drops) was added, and the mixture was gently refluxed for 4−6 h. The mixture was concentrated to half volume at reduced pressure and cooled to room temperature to complete precipitation. The product was recrystalized from absolute ethanol and collected by vacuum filtration and washed by ethanol followed by diethyl ether. Yield 66%. Anal. Calcd for $C_{15}H_{15}N_5O_2S$: C, 51.9; H, 4.9; N, 20.2; S, 9.1%. Found: C, 52.3; H, 4.8, N, 19.3; S, 8.2%. IR (cm^{-1}) 3072w, 1665s, 1611w, 1578w, 1520s, 1471s, 1438w, 1341s, 1308m, 1283m, 1245m, 1169w, 1090m, 977m, 919w, 859w, 820w, 737s, 700m, 675s, 640w, 614m. ^{1}H NMR (DMSO-d_6): δ 8.78 (dt, 1H), 8.5−8.39 (dd, 1H), 8.12 (dd, 2H), 7.86−7.70 (dd, 4H), 3.35 (s, 3H), 3.09 (s, 3H).

General Synthesis of $Fe^{II}(BpT)_2$ Complexes. All ferrous complexes from this series were prepared by the following general method. The appropriate 2-benzoylpyridine thiosemicarbazone (3.5 mmol) was dissolved in EtOH (15 mL), and Et_3N (0.35 g, 3.4 mmol) was added followed by $Fe(ClO_4)_2 \cdot 6H_2O$ (0.64 g, 1.7 mmol). The mixture was gently refluxed for 30 min. The reaction was done under nitrogen. When the mixture was cooled, the green product was filtered off and washed with ethanol and then diethyl ether.

$[Fe(Bp4mT)_2] \cdot 0.5H_2O$. Yield 80%. Anal. ($C_{28}H_{27}FeN_8O_{0.5}S_2$) C, H, N, S. IR ($cm^{-1}$) 3365w, 1589w, 1502s, 1476w, 1425s, 1391s, 1339s, 1232m, 1199m, 1152s, 1014m, 962w, 815w, 772s, 743s, 699s, 658m. Electronic spectrum (MeOH): λ_{max} (nm) (ϵ, L mol^{-1} cm^{-1}) 640 (13 600), 382 (40 800).

$Fe(Bp44mT)_2$. Yield 76%. Anal. Calcd for $C_{30}H_{30}FeN_8S_2$: C, 57.9; H, 4.9; N, 18.0; S, 10.3%. Found: C, 57.1; H, 4.9; N, 18.0; S, 10.3%. IR (cm^{-1}) 2917w, 1586w, 1515s, 1446w, 1421w, 1386s, 1297s, 1234s, 1140s, 1012m, 963w, 920s, 817w, 770s, 741s, 695s,

632s. Electronic spectrum (MeOH): λ_{max} (nm) (ϵ, L mol^{-1} cm^{-1}) 644 (7900), 395 (25 900).

Fe(Bp4eT)$_2$. Yield 67%. Anal. Calcd for $C_{30}H_{30}FeN_8S_2$: C, 57.9; H, 4.9; N, 18.0; S, 10.3. Found: C, 57.5; H, 4.8; N, 18.0; S, 9.7%. IR (cm^{-1}) 3023w, 1590w, 1527s, 1503w, 1449w, 1423m, 1380s, 1333w, 1283w, 1254s, 1198w, 1150w, 1113w, 1087s, 1047m, 1014m, 963w, 920w, 874w, 826w, 771s, 741s, 691s, 645s. Electronic spectrum (MeOH): λ_{max} (nm) (ϵ, L mol^{-1} cm^{-1}) 641 (12 700), 382 (37 600).

[Fe(Bp4aT)$_2$]·3H$_2$O. Yield 77%. Anal. Calcd for $C_{32}H_{36}FeN_8O_3S_2$: C, 54.8; H, 5.2; N, 16.0; S, 9.1%. Found: C, 54.5; H, 4.4; N, 16.0, S, 9.1%. IR (cm^{-1}) 3201w, 1642w, 1593w, 1538w, 1503s, 1407s, 1346w, 1327m, 1307w, 1255w, 1227m, 1189m, 1145w, 1080s, 1017w, 998w, 952w, 909w, 847w, 775s, 747s, 697s, 648w, 619s. Electronic spectrum (MeOH): λ_{max} (nm) (ϵ, L mol^{-1} cm^{-1}) 642 (7700), 378 (40 800).

[Fe(Bp4pT)$_2$]·H$_2$O. Yield 68%. Anal. Calcd for $C_{38}H_{32}FeN_8OS_2$: C, 62.0; H, 4.4; N, 15.2; S, 8.7. Found: C, 61.9; H, 4.2; N, 15.1; S, 7.9. IR (cm^{-1}) 3051w, 1592m, 1520m, 1492w, 1470m, 1401s, 1335w, 1314w, 1245m, 1205w, 1176m, 1149w, 1112w, 1096w, 1071w, 1014w, 962w, 897w, 772m, 741s, 687s, 615m. Electronic spectrum (MeOH): λ_{max} (nm) (ϵ, L mol^{-1} cm^{-1}) 656 (8630), 391 (21 800).

Fe(BpT)$_2$. Yield 56%. Anal. ($C_{26}H_{22}FeN_8S_2$) C, H, N, S. IR (cm^{-1}) 3109w, 1618s, 1580s, 1509w, 1460w, 1407vs, 1335w, 1304s, 1199s, 1150w, 1123s, 1070w, 1054w, 1011m, 945s, 877w, 815w, 771m, 742s, 694s, 663m. Electronic spectrum (MeOH): λ_{max} (nm) (ϵ, L mol^{-1} cm^{-1}) 641 (7300), 367 (20 600).

General Synthesis of Fe^{II}(NBpT)$_2$ Complexes. The appropriate 2-(3′-nitrobenzoyl)pyridine thiosemicarbazone (1.4 mmol) was dissolved in 10 mL of absolute ethanol and purged with nitrogen. Solid Fe(ClO$_4$)$_2$·6H$_2$O (0.27 g, 0.7 mmol) was directly added with stirring, and the nitrogen purge was continued while Et$_3$N (0.15 g) was added. The mixture was then gently refluxed under nitrogen for 1−2 h. The mixture was allowed to cool to complete precipitation. The green product was collected by vacuum filtration and washed by ethanol followed by ether. The complex, Fe(NBp44mT)$_2$, was not prepared because of the extreme lability of the NBp44mT ligand and its low biological activity.

[Fe(NBp4mT)$_2$]·5H$_2$O. Yield 43%. Anal. Calcd for $C_{30}H_{34}FeN_{10}O_9S_2$: C, 43.4; H, 4.4, N, 18.1; S, 8.3%. Found: C, 43.3; H, 3.7; N, 17.3; S, 7.8%. IR (cm^{-1}) 3360w, 1526s, 1452m, 1396s, 1346vs, 1299w, 1270w, 1208w, 1162m, 1095s, 1040w, 1001w, 905w, 863w, 801w, 780w, 737m, 689s, 621m. Electronic spectrum (MeOH): λ_{max} (nm) (ϵ, L mol^{-1} cm^{-1}) 644 (12 300), 382 (36 200).

[Fe(NBp4eT)$_2$]·2H$_2$O. Yield 67%. Anal. Calcd for $C_{30}H_{28}FeN_{10}O_4S_2$: C, 48.1; H, 4.3; N, 18.7; S, 8.6%. Found: C, 47.9; H, 3.8; N, 17.9; S, 7.9%. IR (cm^{-1}) 3250w, 1591w, 1526s, 1470w, 1442w, 1413s, 1388w, 1345s, 1288m, 1255s, 1198w, 1145s, 1119w, 1088s, 1045w, 1018w, 977w, 920w, 874w, 829w, 794w, 771s, 733m, 682s, 637w. Electronic spectrum (MeOH): λ_{max} (nm) (ϵ, L mol^{-1} cm^{-1}) 641 (5800), 380 (21 800).

[Fe(NBp4aT)$_2$]·3.75H$_2$O. Yield 56%. Anal. Calcd for $C_{30}H_{35.5}FeN_{10}O_{7.75}S_2$: C, 46.2; H, 4.6; N, 17.9; S, 8.2%. Found: C, 46.9; H, 3.6; N, 16.8; S, 7.6%. IR (cm^{-1}) 3217w, 3012w, 1641w, 1591w, 1527vs, 1482w, 1445w, 1409s, 1383w, 1344vs, 1323w, 1290w, 1260m, 1260m, 1197w, 1149s, 1122w, 1091w, 1055w, 1018w, 991w, 974w, 921w, 889w, 875w, 818w, 795w, 775s, 751m, 733m, 710s, 684s, 618m. Electronic spectrum (MeOH): λ_{max} (nm) (ϵ, L mol^{-1} cm^{-1}) 646 (9900), 372 (31 200).

[Fe(NBp4pT)$_2$]·3H$_2$O. Yield 60%. Anal. Calcd for $C_{38}H_{34}FeN_{10}O_7S_2$: C, 52.9; H, 4.0; N, 16.2; S, 7.4%. Found: C, 52.2; H, 3.6; N, 15.9; S, 7.0%. IR (cm^{-1}) 3330w, 1598m, 1530s, 1492s, 1421vs, 1374w, 1346s, 1317w, 1251m, 1207w, 1172w, 1104s, 1039s, 998w, 921w, 904w, 836w, 804w, 778m, 751s, 705w, 688s, 651m, 616s. Electronic spectrum (MeOH): λ_{max} (nm) (ϵ, L mol^{-1} cm^{-1}) 656 (9900), 395 (29 700).

[Fe(NBpT)$_2$]·4H$_2$O. Yield 61%. Anal. Calcd for $C_{26}H_{28}FeN_{10}O_8S_2$: C, 42.86%; H, 3.9; N, 19.2; S, 8.8%. Found: C, 42.0; H, 3.4; N, 18.9; S, 8.0%. IR (cm^{-1}) 3285w, 1595m, 1525s, 1410s, 1342s, 1274w, 1205m, 1136m, 1085m, 1015w, 968w, 905w, 874w, 802w, 774m, 736m, 702m, 685s, 621w. Electronic spectrum (MeOH): λ_{max} (nm) (ϵ, L mol^{-1} cm^{-1}) 643 (5600), 371 (25 300).

General Synthesis of [Fe^{III}(BpT)]$^+$ Complexes. The ferric complexes from this series were prepared by the following general method. The appropriate thiosemicarbazone (3.5 mmol) was dissolved in 15 mL of ethanol, and 0.36 g of Et$_3$N was added to the solution. An amount of 0.81 g (1.7 mmol) of Fe(ClO$_4$)$_3$·6H$_2$O was added, and the mixture was gently refluxed for 30 min. When the mixture was cooled, the dark-brown powder was filtered off and washed with ethanol and then diethyl ether. The Fe^{III} complex of NBp44mT was not prepared because of the extreme lability of this ligand and its low biological activity.

[Fe(Bp4mT)$_2$]ClO$_4$·H$_2$O. Yield 91%. Anal. ($C_{28}H_{28}ClFeN_8O_5S_2$) C, H, N, S. IR (cm^{-1}) 3364w, 1585w, 1552s, 1437s, 1395s, 1343m, 1163m, 1077vs, 783m, 749m, 700s, 620s. Electronic spectrum (MeOH): λ_{max} (nm) (ϵ, L mol^{-1} cm^{-1}) 476 (15 700), 379 (37 300).

[Fe(Bp44mT)$_2$]ClO$_4$·0.5H$_2$O. Yield: 88%. Anal. ($C_{30}H_{31}ClFeN_8O_{4.5}S_2$) C, H, N, S. IR (cm^{-1}) 2919w, 1594w, 1542m, 1510m, 1458m, 1440m, 1395s, 1304s, 1249s, 1152w, 1077vs, 967w, 910s, 779m, 746m, 726m, 696s, 665w, 635w, 619s. Electronic spectrum (MeOH): λ_{max} (nm) (ϵ, L mol^{-1} cm^{-1}) 482 (8300), 395 (21 200).

[Fe(Bp4eT)$_2$]ClO$_4$·0.5H$_2$O. Yield 76%. Anal. Calcd for $C_{30}H_{31}ClFeN_8O_{4.5}S_2$: C, 49.3; H, 4.3; N, 15.3; S, 8.8%. Found: C, 49.3; H, 4.5; N, 14.7; S, 8.2%. IR (cm^{-1}) 2976w, 1595w, 1537s, 1505s, 1421s, 1335s, 1297w, 1261w, 1239w, 1194m, 1151m, 1072vs, 998w, 966w, 781s, 747s, 697s, 672w, 657w, 619s. Electronic spectrum (MeOH): λ_{max} (nm) (ϵ, L mol^{-1} cm^{-1}) 483 (11 600), 381 (32 600).

[Fe(Bp4aT)$_2$]ClO$_4$·2H$_2$O. Yield 89%. Anal. Calcd for $C_{32}H_{34}ClFeN_8O_6S_2$: C, 49.1; H, 4.4; N, 14.3; S, 8.2%. Found: C, 48.6; H, 4.1; N, 14.6; S, 7.9%. IR (cm^{-1}) 3306w, 1595w, 1537s, 1504s, 1414s, 1327m, 1251m, 1193w, 1077s, 997w, 921w, 781m, 747s, 696s, 646w, 618s. Electronic spectrum (MeOH): λ_{max} (nm) (ϵ, L mol^{-1} cm^{-1}) 481 (10 200), 382 (26 700).

[Fe(Bp4pT)$_2$]ClO$_4$. Yield 90%. Anal. Calcd for $C_{38}H_{30}ClFe_8O_4S_2$: C, 55.8; H, 3.7; N, 13.7; S, 7.8%. Found: C, 55.2; H, 3.6%; N, 13.9%; S, 7.0%. IR (cm^{-1}) 3275w, 1594m, 1520w, 1493w, 1472w, 1403s, 1336w, 1315w, 1249m, 1204w, 1177m, 1151w, 1096m, 1071s, 1016w, 964w, 898w, 876w, 843w, 823w, 773w, 743s, 688s, 659w, 618s. Electronic spectrum (MeOH): λ_{max} (nm) (ϵ, L mol^{-1} cm^{-1}) 456 (13 300), 402 (24 900).

[Fe(BpT)$_2$]ClO$_4$. Yield 87%. Anal. Calcd for $C_{26}H_{22}ClFe_8O_4S_2$: C, 46.9; H, 3.3; N, 16.8; S, 9.6% Found: C, 46.5; H, 3.5; N, 16.9; S, 9.1%. IR (cm^{-1}) 3154w, 1613m, 1496m, 1426vs, 1322s, 1205s, 1075s, 953w, 780m, 746m, 722w, 697s, 657w, 621s. Electronic spectrum (MeOH): λ_{max} (nm) (ϵ, L mol^{-1} cm^{-1}) 474 (11 200), 371 (23 800).

General Synthesis of [Fe^{III}(NBpT)]$^+$ Complexes. The appropriate thiosemicarbazone (1.4 mmol) was dissolved in 10 mL of absolute ethanol, and 0.33 g (0.7 mmol) of Fe(ClO$_4$)$_3$·6H$_2$O was directly added as a solid with stirring. Et$_3$N (0.15 g) was added, and the mixture was gently refluxed for 2−3 h. The mixture was allowed to cool to room temperature to complete precipitation. The dark-brown product was collected by vacuum filtration and washed with ethanol followed by diethyl ether.

[Fe(NBp4mT)$_2$]ClO$_4$·2.75H$_2$O. Yield 56%. Anal. Calcd for $C_{28}H_{29.5}ClFeN_{10}O_{10.75}$: C, 40.4; H, 3.6; N, 16.8; S, 7.6%. Found: C, 40.1; H, 3.9; N, 16.4; S, 6.7%. IR (cm^{-1}) 3304w, 1596w, 1529s, 1508m, 1449s, 1396s, 1345s, 1297m, 1263m, 1205m, 1161m, 1073vs, 877w, 806m, 779s, 750w, 736s, 686s, 620s. Electronic spectrum (MeOH): λ_{max} (nm) (ϵ, L mol^{-1} cm^{-1}) 482 (11 300), 381 (31 100).

[Fe(NBp4eT)$_2$]ClO$_4$. Yield 67%. Anal. Calcd for $C_{30}H_{28}ClFeN_{10}O_8S_2$: C, 44.4; H, 3.5; N, 17.3; S, 7.9%. Found: C, 43.8; H, 3.8; N, 16.5; S, 7.6%. IR (cm^{-1}) 3312w, 1296m, 1528s, 1505m, 1419s, 1347s, 1297m, 1257m, 1202m, 1156s, 1078vs, 988w, 930w, 876w, 804w, 779s, 750w, 736s, 687s, 620s. Electronic spectrum (MeOH): λ_{max} (nm) (ϵ, L mol^{-1} cm^{-1}) 484 (9000), 382 (27 700).

[Fe(NBp4aT)$_2$]ClO$_4$·0.5H$_2$O. Yield 60%. Anal. Calcd for $C_{30}H_{29}ClFeN_{10}O_{8.5}S_2$: C, 45.5; H, 3.5; N, 16.6; S, 7.6%. Found:

C, 44.9, H, 3.6; N, 15.9; S, 6.9%. IR (cm^{-1}) 3301w, 1596w, 1527s, 1502m, 1446w, 1412s, 1346s, 1325w, 1298w, 1241s, 1200m, 1152w, 1068vs, 988w, 928w, 877w, 805m, 779s, 750w, 735s, 688s, 620s. Electronic spectrum (MeOH): λ_{max} (nm) (ϵ, L mol^{-1} cm^{-1}) 482 (7800), 381 (29 200).

[Fe(NBp4pT)$_2$]ClO$_4$. Yield 65%. Anal. Calcd for $C_{38}H_{28}ClFeN_{10}O_8S_2$: C, 50.3; H, 3.1; N, 15.4; S, 7.1%. Found: C, 51.1; H, 3.4; N, 15.7; S, 6.6%. IR (cm^{-1}) 3075w, 1597m, 1528s, 1495s, 1420s, 1345s, 1253m, 1208w, 1186w, 1074vs, 990w, 904w, 799w, 780w, 750s, 735m, 688s, 620s. Electronic spectrum (MeOH): λ_{max} (nm) (ϵ, L mol^{-1} cm^{-1}) 456 (12 300), 411 (37 900).

[Fe(NBpT)$_2$]ClO$_4$·1.25H$_2$O. Yield 55%. Anal. Calcd for $C_{26}H_{22.5}ClFe_{10}O_{9.25}S_2$: C, 40.1; H, 3.0; N, 18.0; S, 8.3%. Found: C, 41.0; H, 3.5; N, 17.0; S, 7.5%. IR (cm^{-1}) 3284w, 1615s, 1527s, 1493s, 1428s, 1345s, 1223s, 1274w, 1209s, 1149s, 1081vs, 964w, 874w, 806s, 784s, 755w, 724m, 702m, 689m, 623s. Electronic spectrum (MeOH): λ_{max} (nm) (ϵ, L mol^{-1} cm^{-1}) 480 (7500), 364 (18 200).

Biological Studies. Cell Culture. The human SK-N-MC neuroepithelioma and MRC-5 fibroblast cell lines were obtained from the American Type Culture Collection (ATCC; Rockville, MD). The cells were grown as described.[41,49,69]

Preparation of ^{59}Fe Transferrin. Human transferrin (Tf) (Sigma) was labeled with ^{59}Fe (Dupont NEN, MA) to produce ^{59}-Fe$_2$-Tf, as previously reported.[69,70]

Effect of Chelators on Cellular Iron Metabolism. Briefly, SK-N-MC cells were used to study the ability of the chelators to induce ^{59}Fe mobilization from prelabeled cells and prevent ^{59}Fe uptake from ^{59}Fe-Tf. These cells were chosen because their Fe metabolism is well characterized and the chelation efficacy of a wide variety of chelators has been assessed using this cell type.[17,26,41,49,50,60,71]

^{59}Fe Efflux from SK-N-MC Cells. Iron efflux experiments examining the ability of various chelators to mobilize ^{59}Fe from SK-N-MC cells were performed using established techniques.[41,72] Briefly, following prelabeling of cells with ^{59}Fe-Tf (0.75 μM) for 3 h at 37 °C, the cultures were washed four times with ice-cold PBS and subsequently reincubated for 3 h at 37 °C with each chelator (50 μM) or medium alone (control). The overlying media containing released ^{59}Fe were then separated from the cells and placed into γ-counting tubes. Radioactivity was measured in both the cell pellet and supernatant using a γ-scintillation counter (Wallac Wizard 3; Turku, Finland).

Effect of Chelators at Preventing ^{59}Fe Uptake from Tf. The ability of the chelator to prevent cellular ^{59}Fe uptake from Tf was examined using standard techniques.[71,17] Briefly, cells were incubated with ^{59}Fe-Tf (0.75 μM) for 3 h at 37 °C in the presence of each of the chelators (50 μM) or the medium alone (control). The cells were then washed four times with ice-cold PBS, and internalized ^{59}Fe was determined by placing the culture plates on ice and incubating the cell monolayer with the general protease, pronase (1 mg/mL, Sigma), for 30 min at 4 °C.[69,70] The cells were then removed from the monolayer using a plastic spatula and centrifuged for 1 min at 14 000 rpm. The resulting supernatant represents membrane-bound ^{59}Fe-Tf that was released by the protease, while the internalized ^{59}Fe is the pronase-insensitive fraction.[69,70]

Effect of the Chelators on Cellular Proliferation. This was examined using the MTT (3-(4,5-dimethylthiazol-2-yl)-2,5-diphenyltetrazolium) assay by standard methods.[41,49] MTT color formation was directly proportional to the number of viable cells measured by Trypan blue staining.[41]

Ascorbate Oxidation Assay. An established protocol was used to measure ascorbate oxidation.[2,10,27,60,73] Briefly, ascorbic acid (100 μM) was prepared immediately prior to an experiment and incubated in the presence of Fe^{III} (10 μM, added as $FeCl_3$), a 50-fold molar excess of citrate (500 μM), and the chelator (1−60 μM). Absorbance at 265 nm was measured after 10 and 40 min at room temperature, and the decrease of intensity between these time points was calculated.[60,73]

Benzoate Hydroxylation. This assay employs benzoate as a hydroxyl radical scavenger to generate fluorescent salicylate as a product (308 nm excitation and 410 nm emission) using a standard protocol.[10,27,60,73] Briefly, benzoic acid (1 mM) was incubated for 1 h at room temperature in 10 mM disodium hydrogen phosphate (pH 7.4) with 5 mM hydrogen peroxide, the Fe chelator (3−180 μM), and Fe^{III} (30 μM, added as $FeCl_3$). All solutions were prepared immediately prior to use. The addition of Fe was used to start the reaction, and the solution was kept in the dark prior to measuring the fluorescence using a Perkin-Elmer L550B spectrofluorometer. In these experiments, salicylate was used as a standard and also to determine quenching by the chelators.[60,73]

Statistical Analysis. Experimental data were compared using Student's *t*-test. Results were expressed as the mean or mean ± SD (number of experiments) and considered statistically significant when $p < 0.05$.

Acknowledgment. D.R.R. and P.V.B. thank the Australian Research Council (Grants DP0450001 and DP0773027) for research grant funding. D.R.R. acknowledges the National Health and Medical Research Council of Australia for grant and fellowship support. D.S.K. is the grateful recipient of an Australian Post-Graduate Award from the University of Sydney.

Supporting Information Available: Elemental analysis data and crystallographic results (crystal data, bond lengths, and bond angles) of NBpT and Fe(NBp4eT)$_2$. This material is available free of charge via the Internet at http://pubs.acs.org.

References

(1) Bergeron, R. J.; Huang, G.; Weimar, W. R.; Smith, R. E.; Wiegand, J.; et al. Desferrithiocin analogue based hexacoordinate iron(III) chelators. *J. Med. Chem.* **2003**, *46*, 16−24.

(2) Bergeron, R. J.; Wiegand, J.; McManis, J. S.; Bussenius, J.; Smith, R. E.; et al. Methoxylation of desazadesferrithiocin analogues: enhanced iron clearing efficiency. *J. Med. Chem.* **2003**, *46*, 1470−1477.

(3) Chua, A. C.; Ingram, H. A.; Raymond, K. N.; Baker, E. Multidentate pyridinones inhibit the metabolism of nontransferrin-bound iron by hepatocytes and hepatoma cells. *Eur. J. Biochem.* **2003**, *270*, 1689−1698.

(4) Buss, J. L.; Torti, F. M.; Torti, S. V. The role of iron chelation in cancer therapy. *Curr. Med. Chem.* **2003**, *10*, 1021−1034.

(5) Turner, J.; Koumenis, C.; Kute, T. E.; Planalp, R. P.; Brechbiel, M. W.; et al. Tachpyridine, a metal chelator, induces G2 cell-cycle arrest, activates checkpoint kinases, and sensitizes cells to ionizing radiation. *Blood* **2005**, *106*, 3191−3199.

(6) Torti, S. V.; Torti, F. M.; Whitman, S. P.; Brechbiel, M. W.; Park, G.; et al. Tumor cell cytotoxicity of a novel metal chelator. *Blood* **1998**, *92*, 1384−1389.

(7) Regino, C. A.; Torti, S. V.; Ma, R.; Yap, G. P.; Kreisel, K. A.; et al. *N*-Picolyl derivatives of Kemp's triamine as potential antitumor agents: a preliminary investigation. *J. Med. Chem.* **2005**, *48*, 7993−7999.

(8) Larrick, J. W.; Cresswell, P. Modulation of cell surface iron transferrin receptors by cellular density and state of activation. *J. Supramol. Struct.* **1979**, *11*, 579−586.

(9) Cooper, C. E.; Lynagh, G. R.; Hoyes, K. P.; Hider, R. C.; Cammack, R.; et al. The relationship of intracellular iron chelation to the inhibition and regeneration of human ribonucleotide reductase. *J. Biol. Chem.* **1996**, *271*, 20291−20299.

(10) Chaston, T. B.; Lovejoy, D. B.; Watts, R. N.; Richardson, D. R. Examination of the antiproliferative activity of iron chelators: multiple cellular targets and the different mechanism of action of triapine compared with desferrioxamine and the potent pyridoxal isonicotinoyl hydrazone analogue 311. *Clin. Cancer Res.* **2003**, *9*, 402−414.

(11) Nyholm, S.; Mann, G. J.; Johansson, A. G.; Bergeron, R. J.; Graslund, A.; et al. Role of ribonucleotide reductase in inhibition of mammalian cell growth by potent iron chelators. *J. Biol. Chem.* **1993**, *268*, 26200−26205.

(12) Le, N. T. V.; Richardson, D. R. Iron chelators with high antiproliferative activity up-regulate the expression of a growth inhibitory and metastasis suppressor gene: a novel link between iron metabolism and proliferation. *Blood* **2004**, *104*, 2967−2975.

(13) Nurtjahja-Tjendraputra, E.; Fu, D.; Phang, J.; Richardson, D. R. Iron chelation regulates cyclin D1 expression via the proteasome: a link to iron deficiency-mediated growth suppression. *Blood* **2007**, *109*, 4045−4054.

(14) Fu, D.; Richardson, D. R. Iron chelation and regulation of the cell cycle: two mechanisms of post-transcriptional regulation of the universal cyclin-dependent kinase inhibitor $p21^{CIP1/WAF1}$ by iron depletion. *Blood* [Online early access]. DOI: 10.1182/blood-2007-03-076737. Published online 2007. http://bloodjournal.hematologylibrary.org/cgi/content/abstract/blood-2007-03-076737v1.

(15) Kalinowski, D. S.; Richardson, D. R. The evolution of iron chelators for the treatment of iron overload disease and cancer. *Pharmacol. Rev.* **2005**, *57*, 547−583.

(16) Chaston, T. B.; Watts, R. N.; Yuan, J.; Richardson, D. R. Potent antitumor activity of novel iron chelators derived from di-2-pyridylketone isonicotinoyl hydrazone involves fenton-derived free radical generation. *Clin. Cancer Res.* **2004**, *10*, 7365−7374.

(17) Yuan, J.; Lovejoy, D. B.; Richardson, D. R. Novel di-2-pyridyl-derived iron chelators with marked and selective antitumor activity: in vitro and in vivo assessment. *Blood* **2004**, *104*, 1450−1458.

(18) Halliwell, B.; Gutteridge, J. M. Oxygen free radicals and iron in relation to biology and medicine: some problems and concepts. *Arch. Biochem. Biophys.* **1986**, *246*, 501−514.

(19) Barnham, K. J.; Masters, C. L.; Bush, A. I. Neurodegenerative diseases and oxidative stress. *Nat. Rev. Drug Discovery* **2004**, *3*, 205−214.

(20) Aouad, F.; Florence, A.; Zhang, Y.; Collins, F.; Henry, C.; et al. Evaluation of new iron chelators and their therapeutic potential. *Inorg. Chim. Acta* **2002**, *339*, 470−480.

(21) Richardson, D. R. Molecular mechanisms of iron uptake by cells and the use of iron chelators for the treatment of cancer. *Curr. Med. Chem.* **2005**, *12*, 2711−2729.

(22) Blatt, J.; Stitely, S. Antineuroblastoma activity of desferoxamine in human cell lines. *Cancer Res.* **1987**, *47*, 1749−1750.

(23) Donfrancesco, A.; Deb, G.; Dominici, C.; Pileggi, D.; Castello, M. A.; et al. Effects of a single course of deferoxamine in neuroblastoma patients. *Cancer Res.* **1990**, *50*, 4929−4930.

(24) Donfrancesco, A.; Deb, G.; Dominici, C.; Angioni, A.; Caniglia, M.; et al. Deferoxamine, cyclophosphamide, etoposide, carboplatin, and thiotepa (D-CECaT): a new cytoreductive chelation-chemotherapy regimen in patients with advanced neuroblastoma. *Am. J. Clin. Oncol.* **1992**, *15*, 319−322.

(25) Estrov, Z.; Tawa, A.; Wang, X. H.; Dube, I. D.; Sulh, H.; et al. In vitro and in vivo effects of deferoxamine in neonatal acute leukemia. *Blood* **1987**, *69*, 757−761.

(26) Becker, E. M.; Lovejoy, D. B.; Greer, J. M.; Watts, R.; Richardson, D. R. Identification of the di-pyridyl ketone isonicotinoyl hydrazone (PKIH) analogues as potent iron chelators and anti-tumour agents. *Br. J. Pharmacol.* **2003**, *138*, 819−830.

(27) Bernhardt, P. V.; Caldwell, L. M.; Chaston, T. B.; Chin, P.; Richardson, D. R. Cytotoxic iron chelators: characterization of the structure, solution chemistry and redox activity of ligands and iron complexes of the di-2-pyridyl ketone isonicotinoyl hydrazone (HP-KIH) analogues. *J. Biol. Inorg. Chem.* **2003**, *8*, 866−880.

(28) Whitnall, M.; Howard, J.; Ponka, P.; Richardson, D. R. A class of iron chelators with a wide spectrum of potent antitumor activity that overcomes resistance to chemotherapeutics. *Proc. Natl. Acad. Sci. U.S.A.* **2006**, *103*, 14901−14906.

(29) Richardson, D. R.; Sharpe, P. C.; Lovejoy, D. B.; Senaratne, D.; Kalinowski, D. S.; et al. Dipyridyl thiosemicarbazone chelators with potent and selective antitumor activity form iron complexes with redox activity. *J. Med. Chem.* **2006**, *49*, 6510−6521.

(30) Kalinowski, D. S.; Richardson, D. R. Future of toxicology−iron chelators and differing modes of action and toxicity: the changing face of iron chelation therapy. *Chem. Res. Toxicol.* **2007**, *20*, 715−720.

(31) Heuer, L.; Schwamborn, M.; Erdelen, C.; Dehne, H. W.; Berg, D.; et al. Preparation of pyridyl acylhydrazones as microbicides. Bayer−Ger Offen Patent DE 4207400, DE 4207492-4207400, 1993.

(32) Joseph, M.; Kuriakose, M.; Kurup, M. R. P.; Suresh, E.; Kishore, A.; et al. Structural, antimicrobial and spectral studies of copper(II) complexes of 2-benzoylpyridine N(4)-phenylthiosemicarbazone. *Polyhedron* **2006**, *25*, 61−70.

(33) Costa, R. F. F.; Rebolledo, A. P.; Matencio, T.; Calado, H. D. R.; Ardisson, J. D.; et al. Metal complexes of 2-benzoylpyridine-derived thiosemicarbazones: structural, electrochemical and biological studies. *J. Coord. Chem.* **2005**, *58*, 1307−1319.

(34) Rebolledo, A. P.; de Lima, G. M.; Gambi, L. N.; Speziali, N. L.; Maia, D. F.; et al. Tin(IV) complexes of 2-benzoylpyridine N(4)-phenylthiosemicarbazone: spectral characterization, structural studies and antifungal activity. *Appl. Organomet. Chem.* **2003**, *17*, 945−951.

(35) West, D. X.; Ives, J. S.; Krejci, J.; Salberg, M. M.; Zumbahlen, T. L.; et al. Copper(II) complexes of 2-benzoylpyridine 4N-substituted thiosemicarbazones. *Polyhedron* **1995**, *14*, 2189−2200.

(36) Perez-Rebolledo, A.; Ayala, J. D.; de Lima, G. M.; Marchini, N.; Bombieri, G.; et al. Structural studies and cytotoxic activity of N(4)-phenyl-2-benzoylpyridine thiosemicarbazone Sn(IV) complexes. *Eur. J. Med. Chem.* **2005**, *40*, 467−472.

(37) Rebolledo, A. P.; Vieites, M.; Gambino, D.; Piro, O. E.; Castellano, E. E.; et al. Palladium(II) complexes of 2-benzoylpyridine-derived thiosemicarbazones: spectral characterization, structural studies and cytotoxic activity. *J. Inorg. Biochem.* **2005**, *99*, 698−706.

(38) Martinez Aguilar, M. T.; Cano Pavon, J. M. 2-Benzoylpyridine-4-phenyl-3-thiosemicarbazone as an analytical reagent for the spectrophotometric determination of iron. *Mikrochim. Acta* **1977**, *2*, 631−637.

(39) Miller, M. C. I.; Stineman, C. N.; Vance, J. R.; West, D. X.; Hall, I. H. The cytotoxicity of copper(II) complexes of 2-acetyl-pyridyl-4N-substituted thiosemicarbazones. *Anticancer Res.* **1998**, *18*, 4131−4139.

(40) Casas, J. S.; Castellano, E. E.; Ellena, J.; Garcia Tasende, M. S.; Sanchez, A.; et al. Compositional and structural variety of diphenyllead(IV) complexes obtained by reaction of diphenyllead dichloride with thiosemicarbazones. *Inorg. Chem.* **2003**, *48*, 2584−2595.

(41) Richardson, D. R.; Tran, E. H.; Ponka, P. The potential of iron chelators of the pyridoxal isonicotinoyl hydrazone class as effective antiproliferative agents. *Blood* **1995**, *86*, 4295−4306.

(42) Edward, J. T.; Chubb, F. L.; Sangster, J. Iron chelators of the pyridoxal isonicotinoyl hydrazone class. Relationship of the lipophilicity of the apochelator to its ability to mobilize iron from reticulocytes in vitro: reappraisal of reported partition coefficients. *Can. J. Physiol. Pharmacol.* **1997**, *75*, 1362−1368.

(43) Garcia-Tojal, J.; Donnadieu, B.; Costes, J. P.; Serra, J. L.; Lezama, L.; et al. Spectroscopic properties of iron-thiosemicarbazone compounds. Structure of $[Fe(C_7H_7N_4S)_2]\cdot 1.25H_2O$. *Inorg. Chim. Acta* **2002**, *333*, 132−137.

(44) Garcia-Tojal, J.; Pizarro, J. L.; Lezama, L.; Arriortua, M. I.; Rojo, T. Spectroscopic and magnetic properties of the pyridine-2-carbaldehyde thiosemicarbazonate iron(III) complexes: $[Fe(C_7H_7N_4S)_2]X\cdot nH_2O$ (X = Cl, ClO_4, NO_3, PF_6). Crystal structure of the hexafluorophosphate compound. *Inorg. Chim. Acta* **1998**, *278*, 150−158.

(45) West, D. X.; Swearingen, J. K.; Valdes-Martinez, J.; Hernandez-Ortega, S.; El-Sawaf, A. K.; et al. Spectral and structural studies of iron(III), cobalt(II,III) and nickel(II) complexes of 2-pyridineformamide N(4)-methylthiosemicarbazone. *Polyhedron* **1999**, *18*, 2919−2929.

(46) Sreekanth, A.; Kurup, M. R. P. Synthesis, EPR and Moessbauer spectral studies of new iron(III) complexes with 2-benzoylpyridine-N(4),N(4)-(butane-1,4-diyl) thiosemicarbazone (HBpypTsc): X-ray structure of $[Fe(BpypTsc)_2]FeCl_4\cdot 2H_2O$ and the free ligand. *Polyhedron* **2004**, *23*, 969−978.

(47) Sreekanth, A.; Fun, H. K.; Kurup, M. R. P. Structural and spectral studies of an iron(III) complex $[Fe(Pranthas)_2][FeCl_4]$ derived from 2-acetylpyridine-N(4),N(4)-(butane-1,4-diyl) thiosemicarbazone (HPranthas). *J. Mol. Struct.* **2005**, *737*, 61−67.

(48) Lovejoy, D. B.; Richardson, D. R. Novel "hybrid" iron chelators derived from aroylhydrazones and thiosemicarbazones demonstrate selective antiproliferative activity against tumor cells. *Blood* **2002**, *100*, 666−676.

(49) Richardson, D. R.; Milnes, K. The potential of iron chelators of the pyridoxal isonicotinoyl hydrazone class as effective antiproliferative agents II: the mechanism of action of ligands derived from salicylaldehyde benzoyl hydrazone and 2-hydroxy-1-naphthylaldehyde benzoyl hydrazone. *Blood* **1997**, *89*, 3025−3038.

(50) Darnell, G.; Richardson, D. R. The potential of iron chelators of the pyridoxal isonicotinoyl hydrazone class as effective antiproliferative agents III: the effect of the ligands on molecular targets involved in proliferation. *Blood* **1999**, *94*, 781−792.

(51) Feun, L.; Modiano, M.; Lee, K.; Mao, J.; Marini, A.; et al. Phase I and pharmacokinetic study of 3-aminopyridine-2-carboxaldehyde thiosemicarbazone (3-AP) using a single intravenous dose schedule. *Cancer Chemother. Pharmacol.* **2002**, *50*, 223−229.

(52) Bernhardt, P. V.; Mattsson, J.; Richardson, D. R. Complexes of cytotoxic chelators from the dipyridyl ketone isonicotinoyl hydrazone (HPKIH) analogues. *Inorg. Chem.* **2006**, *45*, 752−760.

(53) Johnson, D. K.; Pippard, M. J.; Murphy, T. B.; Rose, N. J. An in vivo evaluation of iron-chelating drugs derived from pyridoxal and its analogs. *J. Pharmacol. Exp. Ther.* **1982**, *221*, 399−403.

(54) Richardson, D. R. Cytotoxic analogs of the iron(III) chelator pyridoxal isonicotinoyl hydrazone: effects of complexation with copper(II), gallium(III), and iron (III) on their antiproliferative activities. *Antimicrob. Agents Chemother.* **1997**, *41*, 2061−2063.

(55) Chaston, T. B.; Richardson, D. R. Iron chelators for the treatment of iron overload disease: relationship between structure, redox activity, and toxicity. *Am. J. Hematol.* **2003**, *73*, 200−210.

(56) Ponka, P.; Schulman, H. M.; Wilczynska, A. Ferric pyridoxal isonicotinoyl hydrazone can provide iron for heme synthesis in reticulocytes. *Biochim. Biophys. Acta* **1982**, *718*, 151−156.
(57) Ponka, P.; Schulman, H. M. Acquisition of iron from transferrin regulates reticulocyte heme synthesis. *J. Biol. Chem.* **1985**, *260*, 14717−14721.
(58) Richardson, D. R.; Ponka, P. The iron metabolism of the human neuroblastoma cell: lack of relationship between the efficacy of iron chelation and the inhibition of DNA synthesis. *J. Lab. Clin. Med.* **1994**, *124*, 660−671.
(59) Baker, E.; Page, M.; Torrance, J.; Grady, R. Effect of desferrioxamine, rhodotorulic acid and cholylhydroxamic acid on transferrin and iron exchange with hepatocytes in culture. *Clin. Physiol. Biochem.* **1985**, *3*, 277−288.
(60) Chaston, T. B.; Richardson, D. R. Interactions of the pyridine-2-carboxaldehyde isonicotinoyl hydrazone class of chelators with iron and DNA: implications for toxicity in the treatment of iron overload disease. *J. Biol. Inorg. Chem.* **2003**, *8*, 427−438.
(61) Verma, P. S.; Saxena, R. C. Cyclic voltammetric studies of certain industrially potential iron chelate catalysts. *Fresenius' J. Anal. Chem.* **1997**, *357*, 56−60.
(62) Aguirre, M. J.; Isaacs, M.; Armijo, F.; Basaez, L.; Zagal, J. H. Effect of the substituents on the ligand of iron phthalocyanines adsorbed on graphite electrodes on their activity for the electrooxidation of 2-mercaptoethanol. *Electroanalysis* **2002**, *14*, 356−362.
(63) Chambers, J.; Eaves, B.; Parker, D.; Claxton, R.; Ray, P. S.; et al. Inductive influence of 4′-terpyridyl substituents on redox and spin state properties of iron(II) and cobalt(II) bis-terpyridyl complexes. *Inorg. Chim. Acta* **2006**, *359*, 2400−2406.
(64) Lanznaster, M.; Neves, A.; Bortoluzzi, A. J.; Assumpcao, A. M. C.; Vencato, I.; et al. Electronic effects of electron-donating and -withdrawing groups in model complexes for iron-tyrosine-containing metalloenzymes. *Inorg. Chem.* **2006**, *45*, 1005−1011.
(65) Hands, A. R.; Katritzky, A. R. N-Oxides and related compounds. XI. Mononitration of 2-, 3-, and 4-phenyl- and 2-, and 4-benzylpyridine 1-oxide. *J. Chem. Soc.* **1958**, 1754−1762.
(66) De Meulenaer, J.; Tompa, H. The absorption correction in crystal structure analysis. *Acta Crystallogr.* **1965**, *19*, 1014−1018.
(67) Rae, A. D. RAELS. *A Comprehensive Constrained Least Squares Refinement Program*; University of New South Wales: New South Wales, Australia, 1996.
(68) Johnson, C. K. *ORTEP-II*; Oak Ridge National Laboratory: Oak Ridge, TN, 1976.
(69) Richardson, D. R.; Baker, E. The uptake of iron and transferrin by the human malignant melanoma cell. *Biochim. Biophys. Acta* **1990**, *1053*, 1−12.
(70) Richardson, D. R.; Baker, E. Intermediate steps in cellular iron uptake from transferrin. Detection of a cytoplasmic pool of iron, free of transferrin. *J. Biol. Chem.* **1992**, *267*, 21384−21389.
(71) Becker, E.; Richardson, D. R. Development of novel aroylhydrazone ligands for iron chelation therapy: 2-pyridylcarboxaldehyde isonicotinoyl hydrazone analogs. *J. Lab. Clin. Med.* **1999**, *134*, 510−521.
(72) Baker, E.; Richardson, D.; Gross, S.; Ponka, P. Evaluation of the iron chelation potential of hydrazones of pyridoxal, salicylaldehyde and 2-hydroxy-1-naphthylaldehyde using the hepatocyte in culture. *Hepatology* **1992**, *15*, 492−501.
(73) Dean, R. T.; Nicholson, P. The action of nine chelators on iron-dependent radical damage. *Free Radical Res.* **1994**, *20*, 83−101.

JM070445Z